

# Characterizing two-timescale nonlinear dynamics using finite-time Lyapunov exponents and vectors<sup>☆</sup>

K.D. Mease<sup>a,1,\*</sup>, U. Topcu<sup>a,2</sup>, E. Aykutluğ<sup>a,2</sup>, M. Maggia<sup>a,2</sup>

<sup>a</sup>*Department of Mechanical and Aerospace Engineering, University of California, Irvine, CA 92697 USA*

## Abstract

Finite-time Lyapunov exponents and vectors are used to define and diagnose boundary-layer type, two-timescale behavior in the tangent linear dynamics and to determine the associated manifold structure in the flow of a finite-dimensional nonlinear autonomous dynamical system. Two-timescale behavior is characterized by a slow-fast splitting of the tangent bundle for a state space region. The slow-fast splitting is defined using finite-time Lyapunov exponents and vectors, guided by the asymptotic theory of partially hyperbolic sets, with important modifications for the finite-time case; for example, finite-time Lyapunov analysis relies more heavily on the Lyapunov vectors due to their relatively fast convergence compared to that of the corresponding exponents. The splitting is used to locate points on normally hyperbolic center manifolds. Determining manifolds from tangent bundle structure is more generally applicable than approaches, such as the singular perturbation method, that require special normal forms or other *a priori* knowledge. The use, features, and accuracy of the approach are illustrated via several detailed examples.

**Keywords:** nonlinear dynamics, multiple timescales, slow manifold, center manifold, finite-time Lyapunov exponents and vectors

## 1. Introduction

The flow of a finite-dimensional autonomous nonlinear dynamical system with multiple timescales may have manifold structure. Characterizing this structure can facilitate simplified analysis and computation, and lead to greater understanding of the system behavior. The relevant timescales are most generally in the linear variational dynamics, i.e., tangent linear dynamics. Our objective is to diagnose two-timescale behavior in tangent linear dynamics with slow dynamics and both stable and unstable fast dynamics, and to compute the associated manifold structure in the flow of the nonlinear system. Because the intent is to analyze finite-time behavior, we first define two-timescale behavior in this context. Though we only directly consider two timescales and normally hyperbolic center manifolds in this paper, the discussion and results are relevant to systems with more than two timescales and also to additional manifold structure, such as the center-stable and center-unstable manifolds relevant to the solution of certain boundary-value problems [4, 23, 49, 58]. We do not consider systems with persistent fast oscillations.

Many of the methods available for computing invariant manifolds (i) operate off the linear structure at an equilibrium point

or a periodic orbit [13], or (ii) require *a priori* knowledge of system coordinates adapted to the manifold structure, e.g. [17, 53], or (iii) require *a priori* knowledge of a manifold that can be analytically or numerically continued to the manifold of interest, e.g. [7, 51]. Our particular application context is flight guidance and control, and our motivation comes from the notable successes of the singular perturbation method [33, 47] in providing insight and facilitating solution approximation with reduced-order models [46]. Geometric singular perturbation theory [15, 30] clarifies the manifold structure in the flow associated with two-timescale behavior. The singular perturbation method is one means of obtaining the manifold structure, but it requires a special coordinate representation, i.e., normal form, with a small parameter, such that the manifold structure for the parameter value of interest can be obtained via matched asymptotic expansions. The singular perturbation method can be viewed as an analytical continuation method; however there is no general systematic method of obtaining the required normal form.

The situation of interest is when two-timescale behavior is suspected in a region of state space, perhaps based on simulation experience, and one wants a means of diagnosing whether or not there are two (or more) disparate timescales and, if there are, a means of characterizing the associated flow structure. In addition to requiring methodology that works away from equilibria and periodic orbits and does not require the singularly perturbed normal form, there is the challenge that, for our target applications, the methodology must be effective when only finite-time behavior is considered. The approach addressed in this paper, which we refer to as finite-time Lyapunov analysis (FTLA), uses finite-time Lyapunov exponents (FTLEs) and the

<sup>☆</sup>This material is based upon work supported by the National Science Foundation under Grants CMMI-0010085 and CMMI-1069331.

\*Corresponding author

Email addresses: kmease@uci.edu (K.D. Mease), utopcu@seas.upenn.edu (U. Topcu), eaykutlu@uci.edu (E. Aykutluğ), mmaggia@uci.edu (M. Maggia)

<sup>1</sup>Professor

<sup>2</sup>Graduate student researcher. U. Topcu is currently a Research Assistant Professor at the University of Pennsylvania. E. Aykutluğ is currently a Postdoctoral Scholar in Earth System Science at U.C. Irvine.

associated vectors (FTLVs), to diagnose two-timescale behavior and characterize the associated tangent bundle structure, and then uses invariance-based orthogonality conditions to locate and compute the associated manifold structure. Orthogonality conditions are used in the intrinsic low-dimensional manifold (ILDM) method [41] in the chemical kinetics context to compute a slow manifold, but the tangent bundle structure is determined by a means other than FTLA. Orthogonality conditions are also used for the computation of invariant manifolds in [51], but the tangent bundle structure is derived from a known neighboring manifold in a numerical continuation scheme.

FTLA is used in different ways in several application contexts. The body of work (e.g., [6, 25, 54, 57]) on characterizing finite-time manifold structure in time-dependent velocity fields has connections with our work, though the target is codimension one manifolds that separate the flow and not two-timescale behavior. In particular the maximum FTLE field is used to determine Lagrangian coherent structures in fluid flows with time-dependent velocity fields, e.g., [12, 24, 57, 59] and to assess the stability of orbits in celestial mechanics [16, 60]. FTLA is used to identify the fastest growing direction(s) of initialization errors in weather predictability theory [8, 37, 61, 62].

FTLA is applied to systems with slow-fast behavior in [2, 43, 44, 52]. In [43], Lyapunov analysis is proposed as a means of diagnosing timescales and suggesting adapted coordinates as an alternative to the singular perturbation approach. In [44], the ILDM and computational singular perturbation (CSP) [34, 35] methods for slow-fast behavior are interpreted geometrically using Fenichel theory and the idea of using FTLE/Vs to improve the ILDM method is proposed. In [2] Lyapunov analysis is applied to periodic and chaotic attractors, as well as slow manifolds, and an approach for computing FTLVs is developed. Lorenz [39] seems to have been the first to use FTLA to analyze a chaotic attractor. In [52], FTLA is used to identify the dimension of the attracting slow manifold along a trajectory. The application of FTLA to the solution of two-timescale boundary value problems related to optimal control is discussed in [4].

The main contribution of the present paper is to extend FTLA to the diagnosis and computation of normally hyperbolic center manifolds. Because the finite time is limited, it is crucial to define the tangent bundle splitting of interest in the fastest converging way and to clarify the finite-time required to accurately approximate the invariant tangent bundle splitting. Guided by the theory of partially hyperbolic sets [27], a finite-time two-timescale set is defined, requiring spatial and temporal uniformity of the spectral gap between the slow and fast FTLEs. A *fast stable–slow–fast unstable* tangent bundle splitting is specified in terms of the FTLVs. The size of the spectral gap dictates the rate of exponential convergence of the tangent bundle splitting toward the desired invariant splitting, providing a guideline for how large the finite-time needs to be. We account for both fast stable and fast unstable behavior and provide orthogonality conditions for approximately computing points on normally hyperbolic center manifolds, whereas previous work on FTLA, with the exception of [4], considered only attracting or repelling center manifolds. Several detailed examples are presented to

illustrate and clarify the approach, and to demonstrate its feasibility and effectiveness in locating and approximating invariant center manifolds.

The paper is organized as follows. In Section 2, we specify the dynamical system to be considered and recall some definitions from geometry. Section 3 provides an overview of the approach and supplements the introduction with background and perspective required to understand the goals and contributions of the present work as well as relations to other work. Section 4 covers Lyapunov analysis: first we define finite-time Lyapunov exponents and vectors (FTLE/Vs) and describe their use for the identification of the tangent space structure; second we briefly describe the asymptotic theory of partially hyperbolic sets; third we address the convergence of the tangent space structure; and fourth we contrast the properties of the FTLE/Vs and their asymptotic counterparts. In Section 5 we define a finite two-timescale set and present the conditions satisfied by points on a finite-time center manifold. The procedure for applying the approach is given in Section 6. Section 7 contains detailed examples. Conclusions are given in Section 8.

## 2. Dynamical System Description and Relevant Geometry

The methodology we develop will be applied to a given coordinate representation of a dynamical system. Denoting the vector of coordinates by  $\mathbf{x} \in \mathbb{R}^n$ , in the standard basis with  $2 \leq n < \infty$ , the  $\mathbf{x}$ -representation of the dynamical system is

$$\dot{\mathbf{x}} = \mathbf{f}(\mathbf{x}), \quad (1)$$

where the vector field  $\mathbf{f} : \mathbb{R}^n \rightarrow \mathbb{R}^n$  is a smooth function. The solution of (1) for the initial condition  $\mathbf{x}$  is denoted by  $\mathbf{x}(t) = \phi(t, \mathbf{x})$ , where  $\phi(t, \cdot) : \mathbb{R}^n \rightarrow \mathbb{R}^n$  is the  $t$ -dependent flow associated with the vector field  $\mathbf{f}$  and  $\phi(0, \mathbf{x}) = \mathbf{x}$ . We assume that  $\phi$  is complete on  $\mathbb{R}^n$  for simplicity, but the methodology developed will only be applied on a subset of the state space and the properties of the flow outside this subset are irrelevant.

The linearized dynamics associated with (1) are

$$\dot{\mathbf{v}} = D\mathbf{f}(\mathbf{x})\mathbf{v} \quad (2)$$

where  $D\mathbf{f} := \partial\mathbf{f}/\partial\mathbf{x}$  and will be analyzed to characterize the timescales. An initial point  $(\mathbf{x}, \mathbf{v})$  is mapped in time  $t$  to the point  $(\mathbf{x}(t), \mathbf{v}(t)) = (\phi(t, \mathbf{x}), \Phi(t, \mathbf{x})\mathbf{v})$  where  $\Phi$  is the fundamental matrix for the linearized dynamics, defined such that  $\Phi(0, \mathbf{x}) = I$ , the  $n \times n$  identity matrix. With this initial condition, we refer to  $\Phi$  as the transition matrix. Geometrically, for a pair  $(\mathbf{x}, \mathbf{v})$ , we view  $\mathbf{v}$  as taking values in the tangent space at  $\mathbf{x}$  denoted by  $T_{\mathbf{x}}\mathbb{R}^n$ . The tangent bundle  $T\mathbb{R}^n$  is the union of the tangent spaces over the state space  $\mathbb{R}^n$  and  $(\mathbf{x}, \mathbf{v})$  is a point in the tangent bundle, with  $\mathbf{v}$  the tangent vector and  $\mathbf{x}$  the base point. We need the interpretation  $(\mathbf{x}, \mathbf{v}) \in T\mathbb{R}^n$ , because the analysis of the linearized dynamics will define a subspace decomposition of the tangent space and the orientation of the subspaces will vary with the base point  $\mathbf{x}$ . Henceforth (2) is called the *tangent linear dynamics*.

We adopt the Euclidean metric for  $\mathbb{R}^n$  and the Euclidean norm to define the length of a tangent vector, i.e., for  $\mathbf{v} \in T_{\mathbf{x}}\mathbb{R}^n$ ,

its length is  $\|\mathbf{v}\| = \langle \mathbf{v}, \mathbf{v} \rangle^{1/2}$  and  $\langle \cdot, \cdot \rangle$  is the standard inner product.

Let  $\mathbf{w}_1, \mathbf{w}_2, \dots, \mathbf{w}_k$ ,  $k \leq n$ , denote vector fields, defined on  $\mathbb{R}^n$ , that vary continuously with  $\mathbf{x}$  and have the property that at each  $\mathbf{x} \in \mathbb{R}^n$ , the vectors  $\mathbf{w}_1(\mathbf{x}), \dots, \mathbf{w}_k(\mathbf{x})$  are linearly independent in  $T_{\mathbf{x}}\mathbb{R}^n$ . Then at each  $\mathbf{x}$ ,  $\Delta(\mathbf{x}) = \text{span}\{\mathbf{w}_1(\mathbf{x}), \dots, \mathbf{w}_k(\mathbf{x})\}$  is a  $k$ -dimensional subspace. If  $k = n$ , then  $\Delta(\mathbf{x}) = T_{\mathbf{x}}\mathbb{R}^n$  and for each  $\mathbf{x}$  the set of vectors provides a basis for  $T_{\mathbf{x}}\mathbb{R}^n$ . If  $k < n$ , then  $\Delta(\mathbf{x})$  is a linear subspace of  $T_{\mathbf{x}}\mathbb{R}^n$ ; let  $\Delta := \bigcup_{\mathbf{x} \in \mathbb{R}^n} \Delta(\mathbf{x})$  denote the subbundle (or distribution) on  $\mathbb{R}^n$ . A subbundle is  $\Phi$ -invariant, if for any  $\mathbf{x} \in \mathbb{R}^n$  and  $\mathbf{v} \in \Delta(\mathbf{x})$ , the property  $\Phi(t, \mathbf{x})\mathbf{v} \in \Delta(\Phi(t, \mathbf{x}))$  holds for all  $t$ . Subbundles  $\Delta_1, \dots, \Delta_m$  allow a splitting of the tangent bundle if  $T\mathbb{R}^n = \Delta_1 \oplus \dots \oplus \Delta_m$ . If each subbundle in the splitting is  $\Phi$ -invariant, then the splitting is a  $\Phi$ -invariant splitting.

Let  $\mathcal{X}$  be a domain in  $\mathbb{R}^n$ . A smooth submanifold  $\mathcal{M} \subset \mathcal{X} \subset \mathbb{R}^n$  of dimension  $m < n$  is  $\mathcal{X}$ -relatively  $\phi$ -invariant, if for each  $\mathbf{x} \in \mathcal{M}$ ,  $\phi(t, \mathbf{x}) \in \mathcal{M}$  for all  $t$  for which  $\phi(t, \mathbf{x})$  has not left  $\mathcal{X}$ . An equivalent requirement for invariance is that  $\mathbf{f}(\mathbf{x}) \in T_{\mathbf{x}}\mathcal{M}$  for all  $\mathbf{x} \in \mathcal{M}$ .

### 3. Overview of Approach

Consider a domain  $\mathcal{X} \subset \mathbb{R}^n$  on which the behavior of (1) on a time interval  $[0, t_f]$  is of interest. The tangent linear dynamics (2) are analyzed to determine if there is a splitting of the tangent bundle into stable, center, and unstable subbundles  $T\mathcal{X} = \mathcal{E}^s \oplus \mathcal{E}^c \oplus \mathcal{E}^u$  of dimensions  $n^s$ ,  $n^c$ , and  $n^u$ , respectively, where the associated exponential rates indicate that, relative to the time interval  $[0, t_f]$ , vectors in the stable subbundle  $\mathcal{E}^s$  decay quickly in forward time, vectors in the unstable subbundle  $\mathcal{E}^u$  decay quickly in backward time, and vectors in the center subbundle evolve slowly. Then postulate that there are corresponding invariant manifolds that organize the flow in the state space on the time interval of interest. For example, an  $n^c$ -dimensional invariant center manifold  $\mathcal{W}^c \subset \mathcal{X}$  can be postulated. At each  $\mathbf{x} \in \mathcal{W}^c$ ,  $T_{\mathbf{x}}\mathcal{W}^c = \mathcal{E}^c(\mathbf{x})$  and  $\mathbf{f}(\mathbf{x}) \in \mathcal{E}^c(\mathbf{x})$ . If  $\{\mathbf{w}_1(\mathbf{x}), \dots, \mathbf{w}_{n-n^c}(\mathbf{x})\}$  is a basis for  $[\mathcal{E}^c(\mathbf{x})]^\perp$ , the orthogonal complement of  $\mathcal{E}^c(\mathbf{x})$ , then a necessary condition for a point  $\mathbf{x} \in \mathcal{W}^c$  is the satisfaction of the orthogonality conditions

$$\langle \mathbf{f}(\mathbf{x}), \mathbf{w}_i(\mathbf{x}) \rangle = 0, \quad i = 1, \dots, n - n^c \quad (3)$$

The orthogonality conditions express that  $\mathbf{f}(\mathbf{x})$  lies in  $T_{\mathbf{x}}\mathcal{W}^c$  at each  $\mathbf{x} \in \mathcal{W}^c$ , i.e., the invariance of  $\mathcal{W}^c$ . The orthogonality conditions for  $\mathbf{f}$  in (3) can be viewed as partial-equilibrium conditions, partial in the sense that the vector field  $\mathbf{f}$  need only be zero when projected into a certain subspace. Similarly, orthogonality conditions can be expressed for points on the center-stable  $\mathcal{W}^{cs}$  and center-unstable  $\mathcal{W}^{cu}$  manifolds.

Figures 1 and 2 show examples of center manifolds in a three-dimensional state space, the relevant geometric objects, and the spectra of characteristic exponents indicating the exponential rates in the tangent linear dynamics, consistent with the geometry. Diagnosing timescale separation and computing such geometric structure, encompassing both the normally attracting center manifold (Fig. 1) and normally hyperbolic center

manifold (Fig. 2) cases, is our goal. Computationally, determining only low-dimensional manifolds may be feasible, but computing selected points on higher-dimensional manifolds is possible and useful (e.g., [4]).

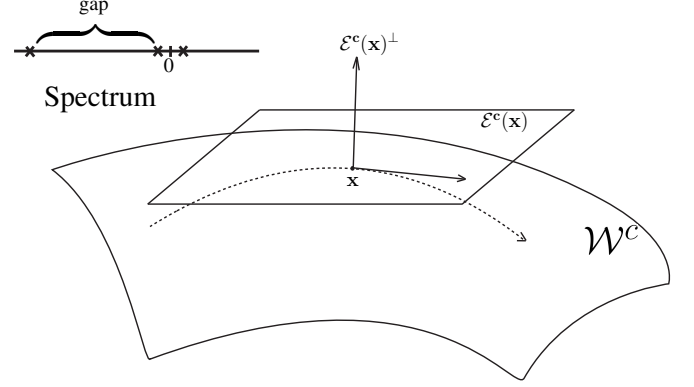


Figure 1: Geometry of a two-timescale 3D system with a 2D normally attracting center manifold.

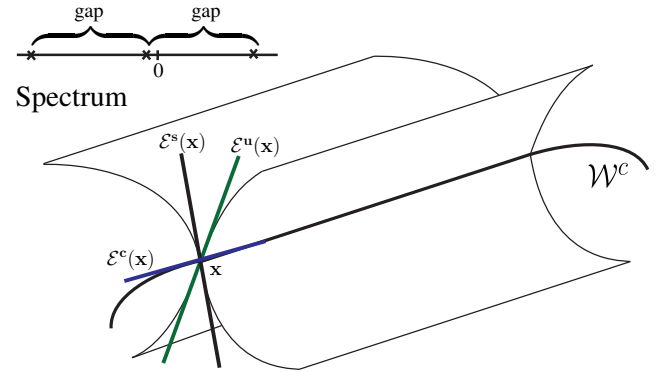


Figure 2: Geometry of a two-timescale 3D system with a 1D normally hyperbolic center manifold.

The theory of partially hyperbolic dynamical systems [27, 28] and Oseledec decompositions [48] guiding our approach focuses on the behavior on the normally hyperbolic manifold, assumes the manifold is a compact invariant set, and considers behavior on an infinite-time interval. For many applications, the manifold of interest is not known a priori, so it must be located by analyzing the behavior over a larger region, and the time interval over which the behavior can be analyzed is finite. In this setting, the approach of determining the tangent bundle splitting and using it to determine the manifold structure in the state space has been pursued.

A feature that distinguishes the approaches that have been taken is the means of determining the timescales and splitting. The eigenvalues and eigenvectors of  $D\mathbf{f}(\mathbf{x})$  are used in the ILDM method [41]. At each point  $\mathbf{x}$  of interest, the eigenvalues provide the timescales and the eigenvectors provide basis vectors for representing the splitting. When applied to a system in the singularly perturbed normal form, the error in determining points on a slow manifold using orthogonality conditions formulated with the eigenvectors of  $D\mathbf{f}(\mathbf{x})$  increases as the

timescale separation decreases and as the curvature of the slow manifold increases [31]. The computational singular perturbation (CSP) method [34, 35, 42] includes an iterative procedure that adjusts the eigenvectors of  $D\mathbf{f}(\mathbf{x})$  to basis vectors that better approximate the slow-fast splitting based on the invariance of these subspaces under the linear flow; see [64] for an error analysis. Eigen-analysis of the symmetric part of  $D\mathbf{f}(\mathbf{x})$  was employed in [9], and eigen-analysis of the symmetric part of a reduced form of  $D\mathbf{f}(\mathbf{x})$  characterizing the directions normal to the vector field was used in [3]. In the chemical kinetics context when the system is dissipative and all trajectories asymptotically approach an equilibrium point, a Lyapunov function is known and a projection to the slow subspace can be derived from it [9].

Finite-time Lyapunov analysis is used in [2, 43, 44]: the FTLEs provide the timescales and the FTLVs provide the basis vectors for representing the splitting. The FTLEs and the FTLVs are the singular values and singular vectors of  $\Phi$  for a propagation time  $T$ . As the propagation time  $T$  goes to zero, the FTLE/Vs approach the eigenvalues/vectors of the symmetric part of  $D\mathbf{f}(\mathbf{x})$  [12]. For Lyapunov regular points, the limits of the FTLEs, as  $T$  goes to infinity, are the asymptotic Lyapunov exponents used in the theory of hyperbolic systems [27, 32]. Thus FTLA can characterize from instantaneous behavior to average behavior over finite to infinite time intervals, depending on the propagation time used.

In [43, 44] FTLA is applied to slow-fast systems to improve the accuracy of slow manifold approximations relative to that of the ILDM method. In [2], in addition to slow manifolds, FTLA is applied to periodic and chaotic attractors which are outside the domain of applicability of the ILDM and CSP methods when the eigenvectors of  $D\mathbf{f}(\mathbf{x})$  either rotate too fast or are complex; see also the earlier work [39] using FTLA for a chaotic attractor. In the present paper we develop FTLA for partially hyperbolic splittings and normally hyperbolic center manifolds.

For the singularly perturbed normal form depending a small parameter  $\varepsilon$ , there is an  $\varepsilon$ -dependent center manifold  $\mathcal{W}^c(\varepsilon)$ , which for  $\varepsilon = 0$  is a manifold composed of equilibrium points [15]. For small  $\varepsilon$ , the flow on  $\mathcal{W}^c(\varepsilon)$  is slow. In this case, the nonlinear dynamics, as well as the tangent linear dynamics, have slow-fast behavior, and it is appropriate to refer to the center manifold as the **slow manifold**. The ILDM and CSP methods were conceived as  $\varepsilon$ -free means, as was the FTLA method in [43, 44], of achieving singular perturbations type results for slow-fast systems; thus it was appropriate to call the center manifold, the slow manifold. However slow-fast behavior in the tangent linear dynamics does not in general imply that the flow on the center manifold is slow,<sup>3</sup> and the approach we develop for normally hyperbolic center manifolds does not require this. Thus we treat a more general class of systems, that includes slow-fast systems, with the common feature that, on the time-interval of interest, there is a fast approach of trajectories to a reduced-order manifold.

<sup>3</sup>The authors thank an anonymous reviewer for stimulating our thinking on this issue.

#### 4. Lyapunov Analysis and Partially Hyperbolic Sets - Finite-Time versus Asymptotic

In this section we present the methodology for characterizing the tangent linear dynamics (2), along trajectories of the nonlinear system (1), that will be used to define and diagnose two-timescale behavior. We refer to this methodology as *Lyapunov analysis*. Because we need to determine, in a limited finite-time, a good approximation of an invariant splitting that in principle requires asymptotic Lyapunov analysis, we need to define the finite-time splitting in a way that will converge as fast as possible towards the desired invariant splitting. We clarify that defining the splitting in terms of FTLVs accomplishes this. In the first subsection, we present a finite-time version of Lyapunov analysis, modeled after the asymptotic version described in Barreira and Pesin [5] and Katok and Hasselblatt [32]. In the second subsection, we describe how asymptotic Lyapunov exponents or vectors can be used to define the ideal invariant splittings; in the third subsection, the convergence rate of a Lyapunov subspace is characterized; and in the final subsection, the products of asymptotic and finite-time Lyapunov analysis are contrasted—in preparation for the finite-time approach presented in the remaining sections. See also [2, 37, 43, 61, 62] for presentations of finite-time Lyapunov analysis.

##### 4.1. Finite-Time Lyapunov Exponents/Vectors and Tangent Space Structure

The forward and backward FTLEs for a vector  $\mathbf{v} \in T_{\mathbf{x}}\mathbb{R}^n$  are given by

$$\mu^\pm(T, \mathbf{x}, \mathbf{v}) := \frac{1}{T} \ln \Lambda^\pm(T, \mathbf{x}, \mathbf{v}) = \frac{1}{T} \ln \frac{\|\Phi(\pm T, \mathbf{x})\mathbf{v}\|}{\|\mathbf{v}\|} \quad (4)$$

where  $T$  is the propagation time, also referred to as the averaging time, and is always taken to be positive whether the propagation is forward or backward. Variables computed by forward and backward propagation are labeled with superscripts  $+$  and  $-$  respectively. For  $\mathbf{v} = \mathbf{0}$ , define  $\mu^+(T, \mathbf{x}, \mathbf{0}) = \mu^-(T, \mathbf{x}, \mathbf{0}) = -\infty$ . The FTLE is the average exponential rate of growth/decay over the time interval  $[0, T]$ .

Discrete forward and backward Lyapunov spectra, for each  $(T, \mathbf{x})$ , can be defined as follows. Define  $\mathbf{I}_i^\pm(T, \mathbf{x})$ ,  $i = 1, \dots, n$ , to be an orthonormal basis of  $T_{\mathbf{x}}\mathbb{R}^n$  with the minimum sum of exponents, i.e., the minimum value of  $\sum_{i=1}^n \mu_i^\pm(T, \mathbf{x}, \mathbf{I}_i^\pm(T, \mathbf{x}))$  over all orthonormal bases [11]. The forward Lyapunov spectrum is the set of exponents corresponding to the minimizing solution, namely,  $\{\mu_i^+(T, \mathbf{x}), i = 1, \dots, n\}$ . The FTLEs are assumed to be in ascending order. The Lyapunov spectrum is unique, though the minimizing basis is not in general.

Geometrically, the unit  $n$ -sphere centered at the origin in  $T_{\mathbf{x}}\mathbb{R}^n$  propagates under the tangent linear dynamics to an  $n$ -dimensional ellipsoid in  $T_{\Phi(T, \mathbf{x})}\mathbb{R}^n$ ; the principal semi-axes of the ellipsoid are  $\exp[\mu_i^+(T, \mathbf{x})T]\mathbf{n}_i^+(T, \mathbf{x})$ ,  $i = 1, \dots, n$  and the unit vectors in  $T_{\mathbf{x}}\mathbb{R}^n$  that evolve to these vectors are respectively  $\mathbf{I}_i^+(T, \mathbf{x})$ ,  $i = 1, \dots, n$ .

The backward Lyapunov spectrum  $\{\mu_i^-, i = 1, \dots, n\}$  consists of the exponents for the unit vectors  $\mathbf{I}_i^-(T, \mathbf{x})$ ,  $i = 1, \dots, n$  in

$T_{\mathbf{x}}\mathbb{R}^n$  that map to principal axes of an  $n$ -ellipsoid in  $T_{\phi(-T,\mathbf{x})}\mathbb{R}^n$ . Descending order is assumed for the backward FTLEs.

The  $\mathbf{l}_i^+(T, \mathbf{x})$  and the  $\mathbf{l}_i^-(T, \mathbf{x})$  vectors, for  $i = 1, \dots, n$ , referred to as forward and backward FTLVs, respectively, will be used to define subspaces in  $T_{\mathbf{x}}\mathbb{R}^n$  associated with different exponential rates. See Fig. 3 for the case of  $n = 2$ .

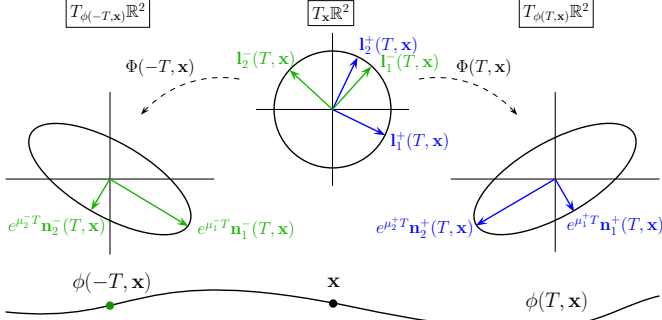


Figure 3: Trajectory of nonlinear system and associated tangent spaces, illustrating the role of the Lyapunov exponents and vectors in the forward and backward propagation of a sphere of tangent vectors. Blue objects correspond to forward propagation, and green objects correspond to backward propagation. The arguments  $(T, \mathbf{x})$  of the FTLE/Vs have been suppressed.

We assume that the FTLEs are always distinct, i.e., non-degenerate. This assumption simplifies the presentation and is needed in slightly stronger form for the subspace convergence proof presented in Appendix A. We note that distinctness is also related to integral separation and the stability of the Lyapunov exponents with respect to perturbations in the linearized system matrix,  $D\mathbf{f}(\mathbf{x})$  [11]. Later we accommodate degeneracies in an initial “transient” phase that is short relative to the time interval under consideration by modifying the assumption to hold for  $T \geq t_s$ , for an appropriate value of the time  $t_s$ .

The following subspaces, for  $i = 1, \dots, n$ , can be defined by the orthonormal FTLVs

$$\begin{aligned} \mathcal{L}_i^+(T, \mathbf{x}) &:= \text{span}\{\mathbf{l}_1^+(T, \mathbf{x}), \dots, \mathbf{l}_i^+(T, \mathbf{x})\}, \\ \mathcal{L}_i^-(T, \mathbf{x}) &:= \text{span}\{\mathbf{l}_i^-(T, \mathbf{x}), \dots, \mathbf{l}_n^-(T, \mathbf{x})\}, \end{aligned} \quad (5)$$

and will be referred to as finite-time Lyapunov subspaces. For any  $i \in \{1, 2, \dots, n\}$ ,  $\mu^+(T, \mathbf{x}, \mathbf{v}) \leq \mu_i^+(T, \mathbf{x})$  for any  $\mathbf{v} \in \mathcal{L}_i^+(T, \mathbf{x})$ . However, for finite  $T$ , there also exist vectors  $\mathbf{v} \in T_{\mathbf{x}}\mathbb{R}^n \setminus \mathcal{L}_i^+(T, \mathbf{x})$  for which  $\mu^+(T, \mathbf{x}, \mathbf{v}) \leq \mu_i^+(T, \mathbf{x})$ . Analogous properties hold for the backward-time exponents and subspaces.

If a collection of  $r \leq n$  linear subspaces of  $T_{\mathbf{x}}\mathbb{R}^n$  can be ordered such that  $\Delta_1(\mathbf{x}) \subset \Delta_2(\mathbf{x}) \subset \dots \subset \Delta_r(\mathbf{x}) = T_{\mathbf{x}}\mathbb{R}^n$  with all inclusions strict, then this collection of nested subspaces defines a *filtration* of  $T_{\mathbf{x}}\mathbb{R}^n$ . The nested sequences of subspaces

$$\{\mathbf{0}\} =: \mathcal{L}_0 \subset \mathcal{L}_1^+(T, \mathbf{x}) \subset \mathcal{L}_2^+(T, \mathbf{x}) \subset \dots \subset \mathcal{L}_n^+(T, \mathbf{x}) = T_{\mathbf{x}}\mathbb{R}^n, \quad (6)$$

$$T_{\mathbf{x}}\mathbb{R}^n = \mathcal{L}_1^-(T, \mathbf{x}) \supset \mathcal{L}_2^-(T, \mathbf{x}) \supset \dots \supset \mathcal{L}_n^-(T, \mathbf{x}) \supset \mathcal{L}_{n+1}^- := \{\mathbf{0}\}, \quad (7)$$

are forward and backward filtrations [5, 32] of  $T_{\mathbf{x}}\mathbb{R}^n$ .

We need both forward and backward filtrations, because their intersections are of particular interest, as motivated by the following. Consider a two-dimensional nonlinear system with

an equilibrium point  $\mathbf{x}_e$ . Assume the linearized dynamics at  $\mathbf{x}_e$  are characterized by distinct eigenvalues  $\lambda_1$  and  $\lambda_2$ , with  $\lambda_1 < \lambda_2 < 0$ , and corresponding unit eigenvectors  $\mathbf{e}_1$  and  $\mathbf{e}_2$ . As  $T \rightarrow \infty$ , the FTLEs at  $\mathbf{x}_e$  approach the eigenvalues, i.e.,  $\mu_1^+(T, \mathbf{x}_e) \rightarrow \lambda_1$  and  $\mu_2^+(T, \mathbf{x}_e) \rightarrow \lambda_2$ , and the first Lyapunov vector approaches the corresponding eigenvector  $\mathbf{l}_1^+(T, \mathbf{x}_e) \rightarrow \mathbf{e}_1$ . The second Lyapunov vector  $\mathbf{l}_2^+(T, \mathbf{x}_e)$  approaches  $\mathbf{e}_1^\perp$ , the vector perpendicular to  $\mathbf{e}_1$ . The subspace  $\mathcal{L}_1^+(T, \mathbf{x}_e)$  thus approaches  $\mathcal{E}^1(\mathbf{x}_e) = \text{span}\{\mathbf{e}_1\}$ , the eigenspace for  $\lambda_1$  as  $T \rightarrow \infty$ , whereas  $\mathcal{L}_2^+(T, \mathbf{x}_e) = T_{\mathbf{x}_e}\mathbb{R}^2$  for any  $T$ . It is desired instead to obtain the invariant splitting  $T_{\mathbf{x}_e}\mathbb{R}^2 = \mathcal{E}^1(\mathbf{x}_e) \oplus \mathcal{E}^2(\mathbf{x}_e)$  where  $\mathcal{E}^2(\mathbf{x}_e) = \text{span}\{\mathbf{e}_2\}$ . However, asymptotically all the vectors not in  $\mathcal{L}_1^+$  have the Lyapunov exponent  $\mu_2^+ = \lambda_2$ ; thus the Lyapunov exponents for forward-time propagation do not distinguish  $\mathcal{E}^2$ . The way to obtain  $\mathcal{E}^2$  is by repeating the same analysis for backward-time propagation; in this case, the situation is reversed: asymptotically  $\mathbf{l}_2^-(T, \mathbf{x}_e) \rightarrow \mathbf{e}_2$  and  $\mathcal{E}^2$  can be distinguished, whereas  $\mathcal{E}^1$  cannot [32, 63].

#### 4.2. Asymptotic Lyapunov Analysis and Partially Hyperbolic Set

We draw from [5, 27] to present the asymptotic theory, covering only those definitions and results that serve to motivate and support our definitions and results for the finite-time case. Asymptotic Lyapunov analysis was introduced in [40] and related to tangent space geometry in [48]. The theory of partially hyperbolic sets is described in [27] where references to the original work are given. The definition of a uniform partially hyperbolic set given next requires exponential bounds uniformly, i.e., on all time intervals for a given trajectory as well as for all trajectories in the set.

**Definition 4.1.** [27] A compact  $\phi$ -invariant set  $\mathcal{Y} \subset \mathbb{R}^n$  is a **uniform partially hyperbolic set**, if there exists a  $\Phi$ -invariant splitting

$$T_{\mathbf{x}}\mathbb{R}^n = \mathcal{E}^s(\mathbf{x}) \oplus \mathcal{E}^c(\mathbf{x}) \oplus \mathcal{E}^u(\mathbf{x}) \quad (8)$$

on  $\mathcal{Y}$  and numbers  $\sigma$ ,  $\nu$ , and  $C$ , with  $0 < \sigma < \nu$  and  $1 \leq C < \infty$ , such that  $\forall t > 0$

$$\begin{aligned} \mathbf{v} \in \mathcal{E}^s(\mathbf{x}) &\Rightarrow \|\Phi(t, \mathbf{x})\mathbf{v}\| \leq Ce^{-\nu t}\|\mathbf{v}\|, \\ \mathbf{v} \in \mathcal{E}^c(\mathbf{x}) &\Rightarrow C^{-1}e^{-\sigma t}\|\mathbf{v}\| \leq \|\Phi(t, \mathbf{x})\mathbf{v}\| \leq Ce^{\sigma t}\|\mathbf{v}\|, \\ \mathbf{v} \in \mathcal{E}^u(\mathbf{x}) &\Rightarrow \|\Phi(-t, \mathbf{x})\mathbf{v}\| \leq Ce^{-\nu t}\|\mathbf{v}\|. \end{aligned} \quad (9)$$

Consistent with the definition, consider for the moment a compact, invariant set  $\mathcal{Y} \subset \mathbb{R}^n$ . When the infinite-time limits ( $T \rightarrow \infty$ ) of the exponents in (4) exist at  $\mathbf{x} \in \mathcal{Y}$  for all  $\mathbf{v} \in T_{\mathbf{x}}\mathbb{R}^n$ , they are denoted by  $\mu^+(\mathbf{x}, \mathbf{v})$  and  $\mu^-(\mathbf{x}, \mathbf{v})$  and the system is said to be, respectively, *forward regular* and *backward regular* at  $\mathbf{x}$ . There are at most  $n$  distinct exponents for the vectors in  $T_{\mathbf{x}}\mathbb{R}^n \setminus \{\mathbf{0}\}$ . Consistent with our assumption for the finite-time case, assume that there are  $n$  distinct exponents, denoted  $\mu_i^+(\mathbf{x})$ ,  $i = 1, \dots, n$  for forward time and  $\mu_i^-(\mathbf{x})$ ,  $i = 1, \dots, n$  for backward time, with the forward exponents in ascending order and the backward exponents in descending order. Lyapunov subspaces are defined by  $\mathcal{L}_i^+(\mathbf{x}) := \{\mathbf{v} \in T_{\mathbf{x}}\mathbb{R}^n : \mu^+(\mathbf{x}, \mathbf{v}) \leq$

$\mu_i^+(\mathbf{x})$  and  $\mathcal{L}_i^-(\mathbf{x}) := \{\mathbf{v} \in T_{\mathbf{x}}\mathbb{R}^n : \mu^-(\mathbf{x}, \mathbf{v}) \leq \mu_i^-(\mathbf{x})\}$ . Forward and backward filtrations are defined as in (6) and (7) using the asymptotic Lyapunov subspaces. The system is *Lyapunov regular* [5] at  $\mathbf{x}$  if (i) it is forward and backward regular at  $\mathbf{x}$ , (ii)  $\mu_i^+(\mathbf{x}) = -\mu_i^-(\mathbf{x})$ ,  $i = 1, \dots, n$ , (iii) the forward and backward filtrations have the same dimensions, (iv) there exists a splitting  $T_{\mathbf{x}}\mathcal{Y} = \mathcal{E}^1(\mathbf{x}) \oplus \dots \oplus \mathcal{E}^n(\mathbf{x})$  into invariant subspaces such that  $\mathcal{L}_i^+(\mathbf{x}) = \mathcal{E}^1(\mathbf{x}) \oplus \dots \oplus \mathcal{E}^i(\mathbf{x})$  and  $\mathcal{L}_i^-(\mathbf{x}) = \mathcal{E}^i(\mathbf{x}) \oplus \dots \oplus \mathcal{E}^n(\mathbf{x})$ ,  $i = 1, \dots, n$ , and (v) for any  $\mathbf{v} \in \mathcal{E}^i(\mathbf{x}) \setminus \{0\}$ ,  $\lim_{t \rightarrow \pm\infty} (1/|t|) \ln \|\Phi(t, \mathbf{x})\mathbf{v}\| = \mu_i^\pm(\mathbf{x})$ . The invariant splitting described in (iv) and (v) is referred to as Oseledec's decomposition.

Next we describe how the Lyapunov exponents and vectors can be used to diagnose and specify a uniform partially hyperbolic set. For the purpose of motivating the finite-time theory presented in the next section, assume the system (1) is Lyapunov regular at all the points of a compact, invariant set  $\mathcal{Y}$ . Suppose we find that at each  $\mathbf{x} \in \mathcal{Y}$ , there are,  $n^s$  large negative exponents,  $n^c$  small in absolute value exponents, and  $n^u$  large positive exponents, with  $n^s + n^c + n^u = n$ . That is, uniformly in  $\mathbf{x}$ , there is a splitting of the forward Lyapunov spectrum  $sp^+(\mathbf{x})$  of the form  $sp^+(\mathbf{x}) := sp^s(\mathbf{x}) \cup sp^c(\mathbf{x}) \cup sp^u(\mathbf{x})$  where  $sp^s(\mathbf{x}) := \{\mu_1^+(\mathbf{x}), \dots, \mu_{n^s}^+(\mathbf{x})\}$ ,  $sp^c(\mathbf{x}) := \{\mu_{n^s+1}^+(\mathbf{x}), \dots, \mu_{n^s+n^c}^+(\mathbf{x})\}$ , and  $sp^u(\mathbf{x}) := \{\mu_{n^s+n^c+1}^+(\mathbf{x}), \dots, \mu_n^+(\mathbf{x})\}$ . We can construct a  $\Phi$ -invariant splitting with

$$\begin{aligned} \mathcal{E}^s(\mathbf{x}) &= \mathcal{L}_{n^s}^+(\mathbf{x}), \\ \mathcal{E}^c(\mathbf{x}) &= \mathcal{L}_{n^s+n^c}^+(\mathbf{x}) \cap \mathcal{L}_{n^s+1}^-(\mathbf{x}), \\ \mathcal{E}^u(\mathbf{x}) &= \mathcal{L}_{n^s+n^c+1}^-(\mathbf{x}). \end{aligned} \quad (10)$$

Although Lyapunov vectors are not normally used to define the subspaces in the asymptotic theory, they can be as follows. Let  $\{\mathbf{l}_i^+(\mathbf{x}), i = 1, \dots, n\}$  denote an orthonormal basis for  $T_{\mathbf{x}}\mathbb{R}^n$  such that  $\{\mathbf{l}_j^+(\mathbf{x}), j = 1, \dots, i\}$  is a basis for  $\mathcal{L}_i^+(\mathbf{x})$  for  $i = 1, \dots, n$ . Let  $\{\mathbf{l}_i^-(\mathbf{x}), i = 1, \dots, n\}$  denote an orthonormal basis for  $T_{\mathbf{x}}\mathbb{R}^n$  such that  $\{\mathbf{l}_j^-(\mathbf{x}), j = i, \dots, n\}$  is a basis for  $\mathcal{L}_i^-(\mathbf{x})$  for  $i = 1, \dots, n$ . When there are  $n$  distinct Lyapunov exponents as we are assuming, it follows that these bases are unique up to multiplication of individual vectors by  $\pm 1$ . These are clearly the orthonormal bases that minimize the sum of the asymptotic exponents over the set of orthonormal bases, and hence the basis vectors are the asymptotic counterparts of the FTLVs.

The final step in specifying the uniform partially hyperbolic set is to define the constants  $\sigma = \sigma_0 + \varepsilon$  and  $\nu = \nu_0 - \varepsilon$  where  $\varepsilon > 0$  is an arbitrarily small constant,

$$\sigma_0 := \max\{|\bar{\mu}^c|, |\underline{\mu}^c|\}, \nu_0 := \min\{-\bar{\mu}^s, \underline{\mu}^u\}, \quad (11)$$

and

$$\begin{aligned} \bar{\mu}^s &= \sup_{\mathbf{x} \in \mathcal{Y}} \mu_{n^s}^+(\mathbf{x}), & \bar{\mu}^c &= \sup_{\mathbf{x} \in \mathcal{Y}} \mu_{n^s+n^c}^+(\mathbf{x}), \\ \underline{\mu}^u &= \inf_{\mathbf{x} \in \mathcal{Y}} \mu_{n^s+n^c+1}^+(\mathbf{x}), & \underline{\mu}^c &= \inf_{\mathbf{x} \in \mathcal{Y}} \mu_{n^s+1}^+(\mathbf{x}). \end{aligned} \quad (12)$$

The bounds are specified in terms of the forward-time exponents  $\mu^+$  as defined in (4), but given the property (ii) of Lyapunov regularity, the backward-time exponents could have been used. For a partially hyperbolic set we must have  $0 < \sigma_0 < \nu_0$ . Then for sufficiently small  $\varepsilon$ , there exists a positive, finite constant  $C$  such that the bounds (9) hold.

#### 4.3. Exponential Lyapunov Subspace Convergence

In this subsection, we relate the finite-time tangent space structure introduced in Section 4.1 to the asymptotic tangent space structure described in Section 4.2. Basically the important subspaces converge exponentially fast to their asymptotic counterparts, and it is this property that makes FTLA viable.

We need to consider the distance between the subspaces  $\mathcal{L}_j^+(T_1, \mathbf{x})$  and  $\mathcal{L}_j^+(T_2, \mathbf{x})$  in  $T_{\mathbf{x}}\mathbb{R}^n$ . For any value of  $j$  in the index set  $\{1, 2, \dots, n\}$ , let  $L_j^+(T, \mathbf{x})$  denote the matrix whose columns are the Lyapunov vectors  $\mathbf{l}_i^+(T, \mathbf{x})$ ,  $i = 1, \dots, j$ , and  $L_j^-(T, \mathbf{x})$  denote the matrix whose columns are the Lyapunov vectors  $\mathbf{l}_i^-(T, \mathbf{x})$ ,  $i = j+1, \dots, n$ . Then the distance between the subspaces  $\mathcal{L}_j^+(T_1, \mathbf{x})$  and  $\mathcal{L}_j^+(T_2, \mathbf{x})$  is

$$\begin{aligned} \text{dist}(\mathcal{L}_j^+(T_1, \mathbf{x}), \mathcal{L}_j^+(T_2, \mathbf{x})) &= \|L_j^+(T_1, \mathbf{x})^T L_j^+(T_2, \mathbf{x})\|_2 \\ &= \|L_j^+(T_2, \mathbf{x})^T L_j^+(T_1, \mathbf{x})\|_2. \end{aligned} \quad (13)$$

This result is a special case of Theorem 2.6.1 in [20], page 76, and the facts that the columns of  $L_j^+(T, \mathbf{x})$  provide an orthogonal basis for  $\mathcal{L}_j^+(T, \mathbf{x})$  and the columns of  $L_j^-(T, \mathbf{x})$  are mutually orthogonal to the columns of  $L_j^+(T, \mathbf{x})$ .

At a forward regular point for which there exists  $t_s > 0$  such that for  $T > t_s$  there is a nonzero lower bound  $\Delta\mu_j^+(\mathbf{x})$  on the spectral gap  $\mu_{j+1}^+(T, \mathbf{x}) - \mu_j^+(T, \mathbf{x})$ , for a specific value of  $j$ , the subspace  $\mathcal{L}_j^+(T, \mathbf{x})$  approaches the fixed subspace  $\mathcal{L}_j^+(\mathbf{x})$ , defined in Section 4.2 in terms of the asymptotic Lyapunov exponent  $\mu_j^+(\mathbf{x})$ . It approaches it at an exponential rate characterized, for every sufficiently small  $\Delta T > 0$ , by

$$\text{dist}(\mathcal{L}_j^+(T, \mathbf{x}), \mathcal{L}_j^+(T + \Delta T, \mathbf{x})) \leq K e^{-\Delta\mu_j^+(\mathbf{x}) \cdot T}, \quad (14)$$

for all  $T > t_s$ , where  $K > 0$  is  $\Delta T$  dependent but  $T$  independent. Similarly, as  $T$  increases, the subspace  $\mathcal{L}_k^-(T, \mathbf{x})$  approaches the fixed subspace  $\mathcal{L}_k^-(\mathbf{x})$  at a rate proportional to  $\exp(-\Delta\mu_k^-(\mathbf{x}) \cdot T)$  where  $\Delta\mu_k^-(\mathbf{x})$  is the spectral gap lower bound for backward propagation and  $T > t_s$ . For the technical details see Appendix A.

#### 4.4. Differences Between Finite-Time and Asymptotic Lyapunov Analysis

As discussed in Section 4.2, in the asymptotic setting either Lyapunov exponents or vectors can serve to define the Lyapunov subspaces and tangent space splitting, and the results are equivalent. In contrast, the FTLEs and FTLVs define different tangent space objects. For example, if one defines the  $i^{\text{th}}$  forward finite-time Lyapunov subspace at  $\mathbf{x}$  as  $\mathcal{V}_i^+(T, \mathbf{x}) := \{\mathbf{v} \in T_{\mathbf{x}}\mathbb{R}^n : \mu^+(T, \mathbf{x}, \mathbf{v}) \leq \mu_i^+(T, \mathbf{x})\}$ , one gets not a subspace, but an object with non-zero volume centered on the FTLV-defined Lyapunov subspace  $\mathcal{L}_i^+(T, \mathbf{x})$  (also noted in [6]). To see this, consider the tangent vector  $\mathbf{v} = \mathbf{u} + \beta \mathbf{w}$  in  $T_{\mathbf{x}}\mathbb{R}^n$ , with  $\mathbf{u} \in \mathcal{L}_i^+(T, \mathbf{x})$ ,  $\mathbf{w} \in [\mathcal{L}_i^+(T, \mathbf{x})]^\perp$ , and  $\beta$  a scalar constant. For a given  $T$ , there exist nonzero values of  $\beta$  close enough to zero that  $\mathbf{v}$  will belong to  $\mathcal{V}_i^+(T, \mathbf{x})$ , whereas it does not belong to  $\mathcal{L}_i^+(T, \mathbf{x})$ . Under certain conditions [48], as  $T$  increases,  $\mathcal{L}_i^+(T, \mathbf{x})$  converges to its asymptotic value  $\mathcal{L}_i^+(\mathbf{x})$  and  $\mathcal{V}_i^+(T, \mathbf{x})$  converges to  $\mathcal{L}_i^+(T, \mathbf{x})$  and thus to  $\mathcal{L}_i^+(\mathbf{x})$  as well. Because the FTLV-defined Lyapunov subspace convergence is exponential in  $T$ , while the Lyapunov exponent convergence is

much slower, perhaps proportional to  $1/T$  [19], in the finite-time setting we define the Lyapunov subspaces in terms of the FTLVs.

The asymptotic Lyapunov exponents for Lyapunov regular points exist as limits, are metric independent, are constant on a trajectory, and include a zero exponent associated with the vector field direction. These properties are not shared in general by the FTLEs. The FTLEs depend on  $\mathbf{x}$  and  $T$ ; there need not be a zero exponent associated with the vector field direction. FTLEs can indicate local behavior which, if not uniformly present, would not be indicated by the asymptotic Lyapunov exponents. Another potential feature in the FTLEs is “nonmodal behavior” [55] which has required the introduction of the delayed start time  $t_s \geq 0$  to avoid a brief initial transient, relative to the time interval of interest, during which the FTLEs can be quite different than they will be for even moderate finite times. FTLEs are in general metric dependent. In the present paper, we use the Euclidean metric exclusively, though any Riemannian metric could be used [22, 38, 43]. If finite-time two-timescale behavior is not present in the original metric under consideration, there may be another metric for which there is two-timescale behavior, as noted by Greene and Kim [22].

## 5. Finite-Time Two-Timescale Set and Center Manifold - Theory

We identify the potential for manifold structure in a state-space region by determining if a representative set  $\mathcal{X} \subset \mathbb{R}^n$  is a finite-time uniform two-timescale set. A two-timescale set has a special tangent space structure and allows us to formulate invariance-based orthogonality conditions that would be satisfied at points of center, center-stable, and center-unstable manifolds, if such manifolds are present. For the purpose of defining and diagnosing two-timescale behavior,  $\mathcal{X}$  could be a point or a segment of a trajectory, as examples, but in the search for manifold structure,  $\mathcal{X}$  is typically a domain of the state space. The domain is typically not  $\phi$ -invariant, so it is crucial to clarify what information is required and how much time it takes to resolve it. And because only limited integration time is available, the definition of a finite-time two-timescale set must account for finite-time features that are of no consequence in asymptotic Lyapunov theory.

### 5.1. Finite-Time Two-Timescale Set

Definition 5.1 of a finite-time uniform two-timescale set is guided by Def. 4.1 of a uniformly partially hyperbolic set and consideration of convergence. Several time constants<sup>4</sup> play key roles. The spectral gap  $\Delta\mu$  must be large enough relative to the common available maximum averaging time  $\bar{T}$  that the tangent space splitting can be accurately resolved; hence the convergence time constant  $\Delta\mu^{-1}$  should allow the finite-time subspaces to converge over at least several time constants toward their ideal infinite-time limits. The fast and slow time constants

(i.e., timescales),  $\nu^{-1}$  and  $\sigma^{-1}$ , appear in the bounds that characterize the disparate exponential rates in the tangent linear dynamics, as further interpreted in Section 5.3.

**Definition 5.1.** A set  $\mathcal{X} \subset \mathbb{R}^n$ ,  $n \geq 2$ , is a **uniform finite-time two-timescale set** for (1) with respect to the Euclidean metric, with fast time constant  $\nu^{-1}$  and slow time constant  $\sigma^{-1}$ , and convergence time constant  $\Delta\mu^{-1}$ , resolvable over  $\Delta\mu(\bar{T} - t_s)$  convergence time constants, if there exist positive integers  $n^s$ ,  $n^c$  and  $n^u$ , with  $n^s + n^c + n^u = n$ , a delayed start time  $t_s$ , a cut-off time  $t_c$ , and an available averaging time  $\bar{T}$  with  $0 \leq t_s < t_c \leq \bar{T}$  such that the following three properties are satisfied. We use the notation  $\mathcal{T} = (t_s, \bar{T}]$  and  $\mathcal{T}_c = (t_s, t_c]$ .

1. **Uniform Spectral Gaps** – There exist positive constants  $\alpha$  and  $\beta$  with  $\beta - \alpha > 0$  such that, uniformly on  $\mathcal{T} \times \mathcal{X}$ , the forward and backward Lyapunov spectra are separated by gaps of size  $\Delta\mu = \beta - \alpha$  into  $n^s$ ,  $n^c$  and  $n^u$  dimensional subsets as illustrated in Fig. 4 and specified by

$$\begin{aligned} \mu_{n^s}^+ &\leq -\beta, & -\alpha &\leq \mu_{n^s+1}^+, & \mu_{n^s+n^c}^+ &\leq \alpha, & \beta &\leq \mu_{n^s+n^c+1}^+, \\ -\mu_{n^s}^- &\leq -\beta, & -\alpha &\leq -\mu_{n^s+1}^-, & -\mu_{n^s+n^c}^- &\leq \alpha, & \beta &\leq -\mu_{n^s+n^c+1}^-. \end{aligned} \quad (15)$$

2. **Tangent Bundle Splitting** – On  $\mathcal{X}$ , there is a continuous splitting

$$T_{\mathbf{x}}\mathbb{R}^n = \mathcal{E}^s(\bar{T}, \mathbf{x}) \oplus \mathcal{E}^c(\bar{T}, \mathbf{x}) \oplus \mathcal{E}^u(\bar{T}, \mathbf{x}), \quad (16)$$

where

$$\begin{aligned} \mathcal{E}^s(\bar{T}, \mathbf{x}) &= \mathcal{L}_{n^s}^+(\bar{T}, \mathbf{x}), \\ \mathcal{E}^c(\bar{T}, \mathbf{x}) &= \mathcal{L}_{n^s+n^c}^+(\bar{T}, \mathbf{x}) \cap \mathcal{L}_{n^s+1}^-(\bar{T}, \mathbf{x}), \\ \mathcal{E}^u(\bar{T}, \mathbf{x}) &= \mathcal{L}_{n^s+n^c+1}^-(\bar{T}, \mathbf{x}). \end{aligned} \quad (17)$$

3. **Two Timescales** – There exist positive numbers  $\nu$  and  $\sigma$  with  $\nu > \sigma$  such that at each  $\mathbf{x} \in \mathcal{X}$  for all  $t \in \mathcal{T}_c$

$$\begin{aligned} \mathbf{v} \in \mathcal{E}^s(\bar{T}, \mathbf{x}) &\Rightarrow \begin{cases} \|\Phi(-t, \mathbf{x})\mathbf{v}\| \geq e^{\nu t}\|\mathbf{v}\| \\ \|\Phi(t, \mathbf{x})\mathbf{v}\| \leq e^{-\nu t}\|\mathbf{v}\| \end{cases}, \\ \mathbf{v} \in \mathcal{E}^c(\bar{T}, \mathbf{x}) &\Rightarrow \begin{cases} e^{-\sigma t}\|\mathbf{v}\| \leq \|\Phi(t, \mathbf{x})\mathbf{v}\| \leq e^{\sigma t}\|\mathbf{v}\| \\ e^{-\sigma t}\|\mathbf{v}\| \leq \|\Phi(-t, \mathbf{x})\mathbf{v}\| \leq e^{\sigma t}\|\mathbf{v}\| \end{cases}, \\ \mathbf{v} \in \mathcal{E}^u(\bar{T}, \mathbf{x}) &\Rightarrow \begin{cases} \|\Phi(-t, \mathbf{x})\mathbf{v}\| \leq e^{-\nu t}\|\mathbf{v}\| \\ \|\Phi(t, \mathbf{x})\mathbf{v}\| \geq e^{\nu t}\|\mathbf{v}\| \end{cases}. \end{aligned} \quad (18)$$

It is assumed that  $n^c \geq 1$ . Either  $n^s$  or  $n^u$  can be zero, but not both. For  $n^s = 0$ ,  $\mathcal{E}^s$  is not relevant; similarly, for  $n^u = 0$ ,  $\mathcal{E}^u$  is not relevant.

In Def. 5.1, Property 1 ensures that common gaps in the forward and backward Lyapunov spectra not only exist, but also separate the spectra in a dimensionally consistent manner, a relaxed version of Lyapunov regularity [5]. The consistency between the forward and backward spectra is illustrated in Fig. 4 where the bounds and forward and backward exponents are plotted on aligned different copies of the real line for clarity. The exponents for particular values of  $T$  and  $\mathbf{x}$  are pictured, but note that Property 1 requires this structure for all  $(T, \mathbf{x}) \in \mathcal{T} \times \mathcal{X}$ .

<sup>4</sup>For an exponential function of time,  $e^{\kappa t}$ , the time constant  $|\kappa|^{-1}$  is the time  $t$  at which the function equals  $e^{+1}$  or  $e^{-1}$  as appropriate for the sign of  $\kappa$ .



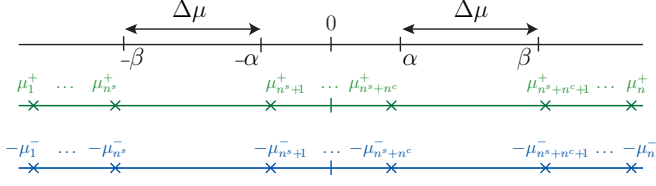


Figure 4: Spectra of forward and backward FTLEs illustrating the gaps.

The symmetry of the gaps with respect to zero is not necessary but is assumed here to simplify the presentation. The use of times up to  $\bar{T}$  means that the computation of the Lyapunov exponents and vectors involves trajectories which, though they begin in  $X$ , extend (unless  $X$  is  $\phi$ -invariant) into the larger set

$$\mathcal{X}_{ext} := \{\mathbf{y} \in \mathbb{R}^n : \mathbf{y} = \phi(t, \mathbf{x}) \text{ or } \mathbf{y} = \phi(-t, \mathbf{x}) \text{ for some } (t, \mathbf{x}) \in \mathcal{T} \times X\}. \quad (19)$$

The delayed start time  $t_s$  provides a grace period over which the FTLE bounds do not have to be satisfied, in order to accommodate “non-modal” behavior [55]; see Section 7.1 for a clarifying example.  $\bar{T}$  is the largest common time over which the uniformity in the exponents holds. We note that because  $\bar{T}$  must apply at each  $\mathbf{x}$ , for a particular  $\mathbf{x}$  larger forward and backward averaging times may be possible; this property is exploited for the example in Section 7.4. Given viable  $\Delta\mu$ ,  $t_s$ , and  $\bar{T}$ , it can be stated that the Lyapunov subspaces are resolvable over at least  $\Delta\mu(\bar{T} - t_s)$  convergence time constants.

In Property 2, the subspaces  $\mathcal{E}^s(\bar{T}, \mathbf{x})$ ,  $\mathcal{E}^c(\bar{T}, \mathbf{x})$  and  $\mathcal{E}^u(\bar{T}, \mathbf{x})$  must uniformly define a splitting of the tangent space – a finite-time version of Oseledec’s decomposition [5, 48]. This condition is a transversality requirement. The continuity of the splitting follows from the continuous dependence of  $\Phi(\bar{T}, \mathbf{x})$  on  $\mathbf{x}$ . We focus on the subspaces for  $\bar{T}$  for the following reason. If the hypotheses of Proposition Appendix A.3 were applicable and the  $T \rightarrow \infty$  limits could be computed, then we could compute the forward and backward Lyapunov subspaces at each point of  $X$  for arbitrarily large averaging times  $T$  and these subspaces would converge to form  $\Phi$ -invariant subbundles [5]. Limited to  $T \leq \bar{T}$  we should use  $T = \bar{T}$  to obtain subspaces that approximate the *ideal* invariant subspaces as closely as possible within the available averaging times. An argument similar to that in the proof of Proposition Appendix A.3 can be used to show that  $\mathcal{L}_{n^s}^+(T, \mathbf{x})$ ,  $\mathcal{L}_{n^s+1}^-(T, \mathbf{x})$ ,  $\mathcal{L}_{n^s+n^c}^+(T, \mathbf{x})$ , and  $\mathcal{L}_{n^s+n^c+1}^-(T, \mathbf{x})$  approach, with increasing  $T$ , fixed subspaces at least at a rate proportional to  $e^{-\Delta\mu T}$ , and consequently so do the subspaces  $\mathcal{E}^s(\bar{T}, \mathbf{x})$ ,  $\mathcal{E}^c(\bar{T}, \mathbf{x})$  and  $\mathcal{E}^u(\bar{T}, \mathbf{x})$ .

Although the bounds  $\alpha$  and  $\beta$  give some indication of the timescales, in Property 3, the action of the transition matrix on vectors in the particular subspaces of the splitting in Property 2 is characterized by exponential bounds. A procedure for determining  $\nu$  and  $\sigma$  is given in Section 6.1. The time interval  $\mathcal{T}_c$  over which the bounds apply is truncated at both ends. The delayed start time avoids the non-modal behavior and the cut-off time  $t_c$  avoids a potential final transient from  $t_c$  to  $\bar{T}$  where a subspace rotates away from the ideal asymptotic subspace it is intended to approximate. For a two-timescale set,  $\nu - \sigma$  is only

required to be positive, but see the interpretation in Subsection 5.3.

## 5.2. Invariant Manifold Approximation

If  $X$ , now assumed to be a domain of  $\mathbb{R}^n$ , is a finite-time uniform two-timescale set, we postulate a corresponding manifold structure for the flow of the nonlinear system (1). The characteristics of the two-timescale set provide the dimensions and orientations of the manifolds. In particular, in the general case where none of the dimensions  $n^s$ ,  $n^c$ , or  $n^u$  is zero, center  $\mathcal{W}^c$ , center-stable  $\mathcal{W}^{cs}$ , and center-unstable  $\mathcal{W}^{cu}$  invariant manifolds can be postulated along with a corresponding invariant splitting  $T_x X = \mathcal{E}^s(\mathbf{x}) \oplus \mathcal{E}^c(\mathbf{x}) \oplus \mathcal{E}^u(\mathbf{x})$ . Points on the postulated invariant manifolds satisfy the conditions

$$\begin{aligned} \mathbf{x} \in \mathcal{W}^c &\Rightarrow \mathbf{f}(\mathbf{x}) \in \mathcal{E}^c(\mathbf{x}) \\ \mathbf{x} \in \mathcal{W}^{cs} &\Rightarrow \mathbf{f}(\mathbf{x}) \in \mathcal{E}^s(\mathbf{x}) \oplus \mathcal{E}^c(\mathbf{x}) \\ \mathbf{x} \in \mathcal{W}^{cu} &\Rightarrow \mathbf{f}(\mathbf{x}) \in \mathcal{E}^c(\mathbf{x}) \oplus \mathcal{E}^u(\mathbf{x}) \end{aligned} \quad (20)$$

Approximating the postulated invariant splitting with our finite-time non-invariant splitting, we can search for points that satisfy the subspace membership conditions (which will be posed as orthogonality conditions in the next section). This leads to the definition of a finite-time center manifold.

**Definition 5.2.** *Given a uniform finite-time two-timescale set  $X$ , a finite-time center manifold is an  $n^c$ -dimensional submanifold of  $X$  denoted  $\mathcal{W}^c(\bar{T})$  such that  $\mathbf{f}(\mathbf{x}) \in \mathcal{E}^c(\bar{T}, \mathbf{x})$  for all  $\mathbf{x} \in \mathcal{W}^c(\bar{T})$ .*

Analogous definitions can be given for the finite-time manifolds  $\mathcal{W}^{cs}(\bar{T})$  and  $\mathcal{W}^{cu}(\bar{T})$ .

## 5.3. Interpretation and Significance

Consider the scenario in which the behavior of a system  $\dot{\mathbf{x}} = \mathbf{f}(\mathbf{x})$  over the time interval  $[0, t_f]$  is of interest. Assume set  $X$  covers the region of state space in which this behavior takes place and has been diagnosed a uniform finite-time two-timescale set with time constants  $\nu^{-1}$  and  $\sigma^{-1}$ . If  $t_f$  is much larger than  $\nu^{-1}$  and smaller than or similar to  $\sigma^{-1}$ , then there is slow-fast behavior in the tangent linear dynamics relative to the time interval of interest.<sup>5</sup> Further, if  $t_s$  and  $\bar{T} - t_c$  are small fractions of  $t_f$ , then the exponential bounds apply on most of the time interval. If an  $n^c$ -dimensional invariant center manifold is present in  $X$  and  $n^u = 0$  ( $n^s = 0$ ), trajectories in a neighborhood of the manifold will approach, during a small fraction of  $t_f$ , the center manifold in forward (backward) time, and one could approximate the behavior over most of the time interval as behavior on the reduced-order manifold. If both  $n^u$  and  $n^s$  are nonzero, then trajectories will approach the invariant center-unstable  $\mathcal{W}^{cu}$  (the invariant center-stable  $\mathcal{W}^{cs}$ ) manifold in forward (backward) time; the example in Section 7.3 illustrates this.

<sup>5</sup>If there is more than one way to separate the FTLE spectra to satisfy Def. 5.1, then the value of  $t_f$  of interest can suggest which way to consider.



Our interest in a center manifold in  $\mathcal{X}$  can be related to interest in a fixed point, in the sense that locating each and analyzing the linearized dynamics provides valuable information about the flow. At a fixed point there is complete equilibrium, whereas on a center manifold there is partial equilibrium. FTLA characterizes the behavior of trajectories in a neighborhood of a normally hyperbolic center manifold, analogous to the role of linear analysis at a hyperbolic fixed point. The non-modal behavior that, for the purpose of locating the center manifold, has been excluded from influencing the FTLEs, via the delayed start time  $t_s$ , can affect the size of the neighborhood [55] and should be considered.

In the remainder of the paper, we focus on computing points on finite-time center manifolds. For the general normally hyperbolic case, this requires obtaining  $[\mathcal{E}^c]^\perp$  by intersecting filtrations from forward and backward integration of the tangent linear dynamics. Points on  $\mathcal{W}^{cu}$  and  $\mathcal{W}^{cs}$  can also be determined using subspace membership conditions and can benefit the solution of certain boundary-value problems [4, 23, 49, 50, 58]. As mentioned earlier, center manifolds need not be slow manifolds. At a point  $\mathbf{x} \in W^c(\bar{T})$ , the exponential bounds for  $\mathcal{E}^c(\bar{T}, \mathbf{x})$  constrain the rate of change in the length of  $\mathbf{f}(\mathbf{x})$  but the FTLA characterization does not constrain the length of  $\mathbf{f}(\mathbf{x})$  and leaves rotational freedom, even fast rotation is possible.

## 6. Finite-Time Two-Timescale Set and Center Manifold - Procedure

If the goal is only to diagnose two-timescale behavior and determine the tangent space structure, then  $\mathcal{X}$  can be any subset of  $\mathbb{R}^n$ . If one also wants to search for a center manifold, then  $\mathcal{X}$  is typically a domain, or a set of grid points on a domain, because it will be necessary to iteratively search for points that satisfy center manifold conditions in a state space region of full dimension. As mentioned, simulation experience with a set of boundary conditions of interest could suggest the domain  $\mathcal{X}$  to explore. Establishing *a priori* that one is searching for a center manifold in a two-timescale set ensures that a uniform splitting exists and can be resolved; however it is also possible to proceed directly to the search and assess the uniformity of the timescales and splitting in the process.

### 6.1. Diagnosing a Finite-Time Two-Timescale Set

The three properties in Def. 5.1 are checked on  $\mathcal{X}$ . To check Property 1, FTLEs are computed to determine if there exist a  $t_s$  and  $\bar{T}$  for which there is a pattern as illustrated in Fig. 4 uniformly in  $\mathbf{x}$  and for all  $T \in \mathcal{T}$ . Regarding uniformity, the individual exponents can vary with  $T$  and  $\mathbf{x}$  as long as there is a sufficiently large uniform gap. However, unless  $\mathcal{X}$  is  $\phi$ -invariant, the set  $\mathcal{X}_{ext}$  (see (19)) grows with  $T$ ; an upper limit on  $T$  may be required to avoid non-uniform behavior. If a uniform spectral gap is present, then the appropriate values of the constants  $n^s, n^c, n^u, t_s, t_c, \bar{T}$  and  $\Delta\mu$  are determined. Based on the initial survey,  $\mathcal{X}$  could be adjusted.

If the tangent space structure is resolvable over at least 3-5 convergence time constants, then the subspaces  $\mathcal{E}^s(\bar{T}, \mathbf{x})$ ,

$\mathcal{E}^c(\bar{T}, \mathbf{x})$  and  $\mathcal{E}^u(\bar{T}, \mathbf{x})$  are constructed and Property 2 is checked. The dimensions of these subspaces sum to  $n$ , but each pair of subspaces must intersect transversely to provide the splitting. We note that the convergence of the subspaces can be checked directly by monitoring the distance between the subspaces with increasing averaging time (illustrated in Section 7).

A means [27] of confirming that an invariant splitting exists close to the splitting (16) uses cones defined as follows. The cone at  $\mathbf{x} \in \mathbb{R}^n$  centered on the subspace  $S(\mathbf{x}) \subset T_{\mathbf{x}}\mathbb{R}^n$  with angle  $\psi \in (0, \pi/2)$  is given by

$$C(\mathbf{x}, S(\mathbf{x}), \psi) := \{\mathbf{v} \in T_{\mathbf{x}}\mathbb{R}^n : \angle(\mathbf{v}, S(\mathbf{x})) < \psi\}, \quad (21)$$

where  $\angle(\mathbf{v}, S(\mathbf{x}))$  is the angle between  $\mathbf{v}$  and its orthogonal projection in  $S(\mathbf{x})$ . One tries to verify that there are families of stable, unstable, center-stable and center-unstable cones

$$\begin{aligned} C^s(\mathbf{x}, \psi) &= C(\mathbf{x}, \mathcal{E}^s(\bar{T}, \mathbf{x}), \psi), & C^u(\mathbf{x}, \psi) &= C(\mathbf{x}, \mathcal{E}^u(\bar{T}, \mathbf{x}), \psi), \\ C^{cs}(\mathbf{x}, \psi) &= C(\mathbf{x}, \mathcal{E}^{cs}(\bar{T}, \mathbf{x}), \psi), & C^{cu}(\mathbf{x}, \psi) &= C(\mathbf{x}, \mathcal{E}^{cu}(\bar{T}, \mathbf{x}), \psi), \end{aligned}$$

where

$$\mathcal{E}^{cs}(\bar{T}, \mathbf{x}) = \mathcal{E}^c(\bar{T}, \mathbf{x}) \oplus \mathcal{E}^s(\bar{T}, \mathbf{x}), \quad \mathcal{E}^{cu}(\bar{T}, \mathbf{x}) = \mathcal{E}^c(\bar{T}, \mathbf{x}) \oplus \mathcal{E}^u(\bar{T}, \mathbf{x}),$$

such that

$$\begin{aligned} \Phi(-t, \mathbf{x})C^s(\mathbf{x}, \psi) &\subset C^s(\phi(-t, \mathbf{x}), \psi), \\ \Phi(t, \mathbf{x})C^u(\mathbf{x}, \psi) &\subset C^u(\phi(t, \mathbf{x}), \psi), \\ \Phi(-t, \mathbf{x})C^{cs}(\mathbf{x}, \psi) &\subset C^{cs}(\phi(-t, \mathbf{x}), \psi), \\ \Phi(t, \mathbf{x})C^{cu}(\mathbf{x}, \psi) &\subset C^{cu}(\phi(t, \mathbf{x}), \psi), \end{aligned}$$

for all  $t \in \mathcal{T}$ . The notation  $\Phi(-t, \mathbf{x})C^s(\mathbf{x}, \psi)$  means the subspace at  $\phi(-t, \mathbf{x})$  are obtained by backward propagation of all the vectors in  $C^s(\mathbf{x}, \psi)$ . For the cone conditions to be satisfied,  $\psi$  must be large enough that the cones contain the actual invariant subspaces. The size of  $\psi$  could be iteratively reduced to get an estimate of how close the splitting is to being invariant.

For each  $\mathbf{x} \in \mathcal{X}$ , the subspaces (17) that define the splitting of the tangent space  $T_{\mathbf{x}}\mathbb{R}^n$  at  $\bar{T}$  can be expressed as the column spans (i.e., range spaces) of the following matrices

$$\begin{aligned} E^s(\bar{T}, \mathbf{x}) &= [\mathbf{I}_1^+(\bar{T}, \mathbf{x}), \dots, \mathbf{I}_{n^s}^+(\bar{T}, \mathbf{x})], \\ E^c(\bar{T}, \mathbf{x}) &= \text{null} \left[ ([E^c(\bar{T}, \mathbf{x})]^\perp)^T \right], \\ E^u(\bar{T}, \mathbf{x}) &= [\mathbf{I}_{n^s+n^c+1}^-(\bar{T}, \mathbf{x}), \dots, \mathbf{I}_n^-(\bar{T}, \mathbf{x})], \end{aligned} \quad (22)$$

$[E^c(\bar{T}, \mathbf{x})]^\perp$  is given in terms of the FTLVs in the next subsection. We have used ‘*null*( $M$ )’ to denote the mapping from matrix  $M$  to an orthonormal matrix whose column span is the null space of the matrix  $M$ .

To check Property 3, we check if  $\nu > \sigma$  after computing the constants  $\nu$  and  $\sigma$  as

$$\nu = \min\{-\bar{\mu}^s, \underline{\mu}^u, \underline{\mu}^s, -\bar{\mu}^u\}, \quad \sigma = \max\{|\underline{\mu}^{c+}|, |\bar{\mu}^{c+}|, |\bar{\mu}^{c-}|, |\underline{\mu}^{c-}|\}$$

where

$$\begin{aligned}\bar{\mu}^s &= \sup_{(T,\mathbf{x}) \in \mathcal{T}_c \times \mathcal{X}} \mu_{n^s}^{s+}(T, \mathbf{x}), & \underline{\mu}^{c+} &= \inf_{(T,\mathbf{x}) \in \mathcal{T}_c \times \mathcal{X}} \mu_1^{c+}(T, \mathbf{x}), \\ \bar{\mu}^u &= \inf_{(T,\mathbf{x}) \in \mathcal{T}_c \times \mathcal{X}} \mu_1^{u+}(T, \mathbf{x}), & \bar{\mu}^{c+} &= \sup_{(T,\mathbf{x}) \in \mathcal{T}_c \times \mathcal{X}} \mu_{n^c}^{c+}(T, \mathbf{x}), \\ \bar{\mu}^s &= \inf_{(T,\mathbf{x}) \in \mathcal{T}_c \times \mathcal{X}} \mu_{n^s}^{s-}(T, \mathbf{x}), & \bar{\mu}^{c-} &= \sup_{(T,\mathbf{x}) \in \mathcal{T}_c \times \mathcal{X}} \mu_1^{c-}(T, \mathbf{x}), \\ \bar{\mu}^u &= \sup_{(T,\mathbf{x}) \in \mathcal{T}_c \times \mathcal{X}} \mu_1^{u-}(T, \mathbf{x}), & \underline{\mu}^{c-} &= \inf_{(T,\mathbf{x}) \in \mathcal{T}_c \times \mathcal{X}} \mu_{n^c}^{c-}(T, \mathbf{x}).\end{aligned}\quad (23)$$

The FTLEs for each subspace as needed in (23) are computed as

$$\mu_i^{j\pm}(T) = \frac{1}{T} \ln \left( \Sigma_{ii}^{j\pm} \right) \quad i = 1, \dots, n^j, j = s, c, u,$$

where the diagonal matrices  $\Sigma^{j\pm}$  are obtained from the singular value decompositions

$$N^{j\pm}(\pm T, \phi(\pm T, \mathbf{x})) \cdot \Sigma^{j\pm}(\pm T, \mathbf{x}) \cdot L^{j\pm}(\pm T, \mathbf{x}) = \Phi(\pm T, \mathbf{x}) E^j(\bar{T}, \mathbf{x}) \quad (24)$$

and the subscript ‘ $ii$ ’ on  $\Sigma$  denotes the  $i^{\text{th}}$  diagonal element of that matrix.

## 6.2. Computing Points on a Finite-Time Center Manifold

Provided that  $\mathcal{X}$  satisfies Def. 5.1, where  $\mathcal{X}$  is now assumed to be a domain of  $\mathbb{R}^n$ , we can look for a normally hyperbolic center manifold in  $\mathcal{X}$ . Within  $\mathcal{X}$ , the points in the set

$$\{\mathbf{x} \in \mathcal{X} : \langle \mathbf{f}(\mathbf{x}), \mathbf{w} \rangle = 0, \forall \mathbf{w} \in [\mathcal{E}^c(\bar{T}, \mathbf{x})]^\perp\} \quad (25)$$

satisfy a necessary condition for being on a finite-time center manifold. Whether or not this set, or a subset of it, is a submanifold of  $\mathcal{X}$  has to be determined to the extent it can from numerical results, which is also the case with the ILDM method [41]. We proceed under the assumption that the set is a manifold that can locally be parametrized by  $n^c$  of the  $n$  system coordinates and represented as a graph. Situations with folded or multiple center manifolds, or where the set is an object of fractal dimension are possible; see [39] for an example of analyzing the case of a fractal attractor, though not characterized as the set (25).

Rather than use eigenvectors of  $D\mathbf{f}(\mathbf{x})$  to form an approximate basis for the orthogonal complement to  $\mathcal{E}^c$  as in the ILDM method [41], we use the appropriate Lyapunov vectors to form the approximate basis as prescribed in the following proposition.

**Proposition 6.1.** *On a uniform finite-time two-timescale set  $\mathcal{X}$ , at each  $\mathbf{x}$ , the vectors*

$$\mathbf{l}_1^-(\bar{T}, \mathbf{x}), \dots, \mathbf{l}_{n^s}^-(\bar{T}, \mathbf{x}), \mathbf{l}_{n^s+n^c+1}^+(\bar{T}, \mathbf{x}), \dots, \mathbf{l}_n^+(\bar{T}, \mathbf{x}) \quad (26)$$

form a basis for  $[\mathcal{E}^c(\bar{T}, \mathbf{x})]^\perp$ .

*Proof:* In Def. 5.1, Property 2, the  $n^c$ -dimensional center subspace is given by  $\mathcal{E}^c(\bar{T}, \mathbf{x}) = \mathcal{L}_{n^s+n^c}^+(\bar{T}, \mathbf{x}) \cap \mathcal{L}_{n^s+1}^-(\bar{T}, \mathbf{x})$ . Using an identity from [29], we have  $[\mathcal{E}^c(\bar{T}, \mathbf{x})]^\perp = [\mathcal{L}_{n^s+1}^-(\bar{T}, \mathbf{x})]^\perp \oplus [\mathcal{L}_{n^s+n^c}^+(\bar{T}, \mathbf{x})]^\perp$ . The proposition then follows from the facts:  $[\mathcal{L}_{n^s+1}^-(\bar{T}, \mathbf{x})]^\perp = \text{span} \{\mathbf{l}_1^-(\bar{T}, \mathbf{x}), \dots, \mathbf{l}_{n^s}^-(\bar{T}, \mathbf{x})\}$  and  $[\mathcal{L}_{n^s+n^c}^+(\bar{T}, \mathbf{x})]^\perp = \text{span} \{\mathbf{l}_{n^s+n^c+1}^+(\bar{T}, \mathbf{x}), \dots, \mathbf{l}_n^+(\bar{T}, \mathbf{x})\}$ . ■

The set (25) is thus the solution set for the system of orthogonality conditions

$$\begin{aligned}\langle \mathbf{f}(\mathbf{x}), \mathbf{l}_i^-(\bar{T}, \mathbf{x}) \rangle &= 0, i = 1, \dots, n^s \\ \langle \mathbf{f}(\mathbf{x}), \mathbf{l}_j^+(\bar{T}, \mathbf{x}) \rangle &= 0, j = n^s + n^c + 1, \dots, n\end{aligned}\quad (27)$$

In order to obtain solutions of the algebraic equations, we designate  $n^c$  components of  $\mathbf{x}$  as independent variables to parameterize the manifold and determine the values of the remaining  $n - n^c$  components, the dependent variables, that satisfy the orthogonality conditions in (25). Because the FTLVs are in numerical form, we use a successive approximation approach described in Section 7.4. This is repeated for a grid on the space of independent variables. The directions of the Lyapunov vectors indicate how to separate the coordinates of  $\mathbf{x}$  into independent and dependent variables, i.e., how to locally parametrize the postulated  $\mathcal{W}^c(\bar{T})$ . The independent variables must be chosen such that their coordinate axes are not parallel to any directions in  $[\mathcal{E}^c]^\perp$ . Different independent variables might be required for different sections of the center manifold.

Consideration of the planar system

$$\dot{\mathbf{x}} = \mathbf{f}(\mathbf{x}) = \mathbf{e}^c(x_1)g(x_1) + \mathbf{e}^s(x_1)h(x_1, x_2) \quad (28)$$

where  $\mathbf{e}^c$  and  $\mathbf{e}^s$  are unit basis vectors for the exact center and stable subspaces and  $g$  and  $h$  are scalar functions, provides some insight into what the accuracy of the finite-time manifold depends on. Assume there is an invariant center manifold given by the solution set for  $h(x_1, x_2) = 0$  and parametrizable by  $x_1$ . For a particular value of  $x_1$ , let unit vector  $\mathbf{w}$  be the approximation of the direction orthogonal to  $\mathbf{e}^c$  at the correct location  $x_2^c$  of the manifold. Assume  $\langle \mathbf{w}, \mathbf{e}^c \rangle = \sin(\varepsilon)$  and  $\langle \mathbf{w}, \mathbf{e}^s \rangle = \sin(\delta + \varepsilon)$ , where  $\varepsilon$  is the angular error in approximating  $\mathbf{e}^c$  and  $\delta$  is the angle between  $\mathbf{e}^c$  and  $\mathbf{e}^s$ . Then the manifold error is

$$\Delta x_2 = -\frac{\sin(\varepsilon)}{\sin(\delta + \varepsilon)} g(x_1) \left( \frac{\partial h}{\partial x_2}(x_1) \right)^{-1} \quad (29)$$

In addition to the subspace error  $\varepsilon$ , the manifold error depends on the angle  $\delta$  between  $\mathbf{e}^c$  and  $\mathbf{e}^s$  and the ratio  $g/(\partial h/\partial x_2)$ .

## 6.3. Numerical Methods for FTLA

Numerical methods for FTLA are addressed in [1, 2, 11, 18, 61] and the references therein. For completeness, the methods used for the computations presented in the next section are described in this subsection. All the computations are done in the Matlab® environment. The numerical integration of the nonlinear state equations and the corresponding linear variational equations is performed with the ‘ode45’ integrator.

The FTLEs and FTLVs associated with an initial state  $\mathbf{x}$  are computed for an averaging time  $T$  either by SVD or QR factorization. Only the computation of the forward-time FTLE/Vs is described, since the computation of the backward-time FTLE/Vs is analogous. The first step of both methods is to integrate the nonlinear state equations from  $t = 0$  to  $t = T$  and save the values of  $\phi(t, \mathbf{x})$  at the  $N$  equally spaced times  $\Delta t, 2\Delta t, \dots, N\Delta t$ , where  $N\Delta t = T$ .

In the SVD method, the transition matrix is computed and then the SVD is applied. The transition matrix is computed by integrating, simultaneously, the nonlinear equations and the associated linear variational equations over each segment of the base space trajectory, with the state initialized with the saved value at the beginning of the segment and the transition matrix initialized with the identity matrix. Using the notation  $\Phi_k^{\Delta t} = \Phi(\Delta t, \phi[(k-1) \cdot \Delta t, \mathbf{x}])$  for  $k = 1, 2, \dots, N$ , the transition matrix is constructed from the transition matrices for the segments as  $\Phi(T, \mathbf{x}) = \Phi_N^{\Delta t} \dots \Phi_2^{\Delta t} \Phi_1^{\Delta t}$ . The resulting transition matrix is then factored as  $\Phi(T, \mathbf{x}) = N^+ \Sigma^+ (L^+)^T$  using the 'svd' command in Matlab<sup>®</sup>. Each FTLE is obtained by  $\mu_i^+(T, \mathbf{x}) = \frac{1}{T} \ln \sigma_i^+$ , where  $\sigma_i$  is the  $i^{\text{th}}$  singular value of  $\Phi$ , the positive square root of the  $i^{\text{th}}$  diagonal element of  $\Sigma^+$ . If this procedure does not produce FTLEs in the ascending order we have assumed in our notation, the FTLEs and associated FTLVs are rearranged to conform. The FTLVs  $\mathbf{l}_i^+(T, \mathbf{x}), i = 1, \dots, n$  are the column vectors of  $L^+$ .

For a given trajectory from  $\mathbf{x}$  to  $\phi(T, \mathbf{x})$ , for a particular  $T$ , we have the option of computing the Lyapunov vectors at  $\mathbf{x}$  and at  $\phi(T, \mathbf{x})$  by forward or backward integration. Because  $\Phi(-T, \phi(T, \mathbf{x})) = \Phi^{-1}(T, \mathbf{x})$ , it follows that  $L^+(T, \mathbf{x}) = N^-(T, \phi(T, \mathbf{x}))$  and  $N^+(T, \mathbf{x}) = L^-(T, \phi(T, \mathbf{x}))$ . As pointed out by others, e.g. in [37], it is best to compute  $L^+(T, \mathbf{x})$  by backward integration from  $\phi(T, \mathbf{x})$  and  $L^-(T, \phi(T, \mathbf{x}))$  by forward integration from  $\mathbf{x}$  so that the vectors and subspaces one is seeking are those to which the linear flow naturally carries the vectors and subspaces. The QR method is based on this strategy.

In the QR method, a segmented approach is also used [11]. For the  $k^{\text{th}}$  segment, after the transition matrix is computed as described in the previous paragraph, the  $Q_{k-1}$  matrix associated with the state at the end of the previous segment is propagated by the transition matrix to the end of the  $k^{\text{th}}$  segment and the  $Q_k R_k$  factorization of the resulting matrix is obtained, as summarized by

$$\Phi_k^{\Delta t} Q_{k-1} = Q_k R_k. \quad (30)$$

This sequence of operations for  $k = 1, \dots, N$  must be initialized by prescribing  $Q_0$ ; typically the identity matrix is used [11, 18]. It then follows that

$$\Phi(T, \mathbf{x}) Q_0 = Q(T, \mathbf{x}) R \quad (31)$$

where  $Q(T, \mathbf{x}) = Q_N$  and  $R = R_N R_{N-1} \dots R_2 R_1$ . For almost every  $Q_0$ , as  $T$  increases,  $Q(T, \phi(T, \mathbf{x}))$  will approach  $N^+(T, \phi(T, \mathbf{x}))$  and the diagonal elements of  $R$  will approach the diagonal elements of  $\Sigma^+$  in the absence of numerical errors. Note that, for any  $T$ , if we choose  $Q_0 = L^+(T, \mathbf{x})$ , then  $Q(T, \mathbf{x}) = N^+(T, \mathbf{x})$ , or equivalently  $Q(T, \mathbf{x}) = L^-(T, \phi(T, \mathbf{x}))$ , and  $R = \Sigma^+$ . In our experience, the QR method is generally more reliable than the SVD method for calculating the FTLE/Vs for longer averaging times. For shorter times, as needed to compute the exponent bounds, the SVD should be used.

## 7. Application Examples

Several application examples are presented to demonstrate the use of the FTLA methodology. The first example provides insight into the start and cut-off times used in Definition

5.1. The angles between the relevant vectors and subspaces are intentionally small to illustrate how the FTLA method handles the consequences. The remaining three examples illustrate the FTLA methodology for 2D, 3D, and 4D systems, the second two involving normally hyperbolic center manifolds. For these examples, the subspaces in the splitting are separated by angles of at least 45 degrees, and the center manifolds are slow manifolds. Given that our initial motivation for developing the FTLA method for determining a slow manifold was to improve the accuracy of the ILDM method in situations where the ILDM method is known to be inaccurate [31], the FTLA method results are compared to the results obtained with the ILDM method. The comparisons thus focus on the differences between using FTLA and analyzing the tangent linear dynamics as if they were time-invariant and how these differences map into manifold errors. Note that other means of improving the results of the ILDM method have been developed, e.g., [45].

### 7.1. Example for Understanding Start and Cut-Off Times

Properties 1 and 3 in Def. 5.1 involve truncating the time interval at the beginning and end, using the start time  $t_s$  and the cut-off time  $t_c$ . The initial transient behavior that is excluded is associated with coordinate-dependent angles between certain subspaces toward which the finite-time subspaces are converging. The final transient behavior that is excluded is produced by the lack of  $\Phi$ -invariance of the finite-time subbundles  $\mathcal{E}^s$ ,  $\mathcal{E}^c$  and  $\mathcal{E}^u$ . To illustrate the behaviors and the roles of the constants  $t_s$  and  $t_c$ , we consider a 7D system,  $\dot{\mathbf{x}} = \mathbf{f}(\mathbf{x})$ , at an equilibrium point  $\mathbf{x}_e$ , i.e., for  $X = \{\mathbf{x}_e\}$ , with

$$D\mathbf{f}(\mathbf{x}_e) = \begin{bmatrix} -5.4 & 1 & 0 & 0 & 0 & 0 & 0 \\ 0 & -5.2 & 0 & 0 & 30 & 0 & 0 \\ 0 & 0 & -0.3 & 0 & 0 & 0 & 10 \\ 0 & 0 & 0 & -0.1 & 0 & 0 & 0 \\ 0 & 0 & 0 & 0 & 0.2 & 0 & 0 \\ 0 & 0 & 0 & 0 & 0 & 4.0 & 8 \\ 0 & 0 & 0 & 0 & 0 & 0 & 4.6 \end{bmatrix}. \quad (32)$$

The triangular form of  $D\mathbf{f}(\mathbf{x}_e)$  allows simple control of the timescales, the important angles, and the degree of dynamic coupling via specification of the diagonal and off-diagonal elements.

Barring numerical errors, in the limit  $\bar{T} \rightarrow \infty$ , the FTLEs will converge to the eigenvalues of  $D\mathbf{f}(\mathbf{x}_e)$ , i.e., the diagonal elements, and the subspaces  $\mathcal{E}^s$ ,  $\mathcal{E}^c$  and  $\mathcal{E}^u$  will converge to the stable, center and unstable eigenspaces, i.e., the subspaces spanned by the appropriate subset of the eigenvectors of  $D\mathbf{f}(\mathbf{x}_e)$  – the stable eigenspace spanned by the eigenvectors for the eigenvalues  $\lambda_1 = -5.4$  and  $\lambda_2 = -5.2$ , the center eigenspace spanned by the eigenvectors for  $\lambda_3 = -0.3$ ,  $\lambda_4 = -0.1$  and  $\lambda_5 = 0.2$  and the unstable eigenspace spanned by the eigenvectors for  $\lambda_6 = 4.0$  and  $\lambda_7 = 4.6$ .

In order to determine the cut-off time  $t_c$ , the FTLEs for the subspaces  $\mathcal{E}^s$ ,  $\mathcal{E}^c$  and  $\mathcal{E}^u$  computed for a finite  $\bar{T}$  ( $\mu_i^{j\pm}, i = 1, \dots, n^j, j = s, c, u$ ) are considered to determine the exponential bounds as described in Section 6.1. For sufficiently large

finite  $\bar{T}$ , the subspaces  $\mathcal{E}^s$ ,  $\mathcal{E}^c$  and  $\mathcal{E}^u$  will closely approximate the corresponding fixed eigenspaces, but when propagated to  $\bar{T}$ , there will be a final boundary-layer in which the subspaces rotate away from the eigenspaces and this will affect the behavior of the FTLEs. For example, the stable eigenspace is asymptotically stable in backward time and unstable in forward time with respect to neighboring equi-dimensional subspaces. Thus, when propagated forward in time, the finite-time approximation  $\mathcal{E}^s$  will rotate away from the stable eigenspace. This is a non-uniform rotation taking place primarily near the time  $\bar{T}$  for which  $\mathcal{E}^s$  was computed. In general  $\mathcal{E}^s$  and  $\mathcal{E}^c$  will rotate toward  $\mathcal{E}^u$  in forward time, and  $\mathcal{E}^c$  and  $\mathcal{E}^u$  will rotate toward  $\mathcal{E}^s$  in backward time. The FTLEs for  $\mathcal{E}^s$ ,  $\mathcal{E}^c$  and  $\mathcal{E}^u$  will be similar to those for their eigenspace counterparts except in cases involving propagation in the unstable direction when the averaging time is near  $\bar{T}$ . Thus we exclude a final transient period long enough to avoid the corresponding deviations in the FTLEs. Figure 5 shows the backward and forward FTLEs for each of the three subspaces for  $\bar{T} = 6.0$ . The final transients are short and the deviations are not large; the final transients that dictate  $t_c = 5.5$  are the ones for the forward and backward propagations of the center subspace. On the other hand, the determination of the start time  $t_s$  comes from the requirement of satisfying properties 1 and 3 of 5.1. Therefore, we will consider both the FTLEs that define the exponential bounds (17) and the FTLEs that define the spectral gap  $\Delta\mu$ . For convenience, we will refer to these two sets of FTLEs as  $\mu_{EB}^\pm$  and  $\mu^\pm$  respectively. The  $\mu_{EB}^\pm$ 's associated with a particular subspace, as functions of  $T$ , will have an initial transient period, if the subspace has dimension greater than one and there is one or more pair of eigenvectors within the eigenspace being approximated that are separated by an angle less than  $90^\circ$  in the coordinates being used. In this example, the angles referred to are those between the eigenvectors that span the stable, center, and unstable eigenspaces. Angles less than  $90^\circ$  are responsible for the funnel-shaped initial transient behavior of the  $\mu_{EB}^\pm$ . For instance, the angle between the two eigenvectors associated with the two largest eigenvalues is  $9.7^\circ$  and the backward  $\mu_{EB}^-$  for  $\mathcal{E}^u$  in the  $T \rightarrow 0$  limit (i.e. the opposites of the eigenvalues of the symmetric part of  $Df(\mathbf{x}_c)$ , which are  $-2.5$  and  $-6.1$ ) are not consistent with the  $\mu^-$  for most averaging times up to  $\bar{T}$ ; this is referred to as non-modal behavior [55]. By excluding a period  $[0, t_s]$  the initial transient behavior is eliminated. A similar argument can be made when considering the FTLEs  $\mu^\pm$ .

Figure 5 shows the FTLEs  $\mu_{EB}^\pm$  used to determine the constants  $\nu$ ,  $\sigma$  as described in Section 6.1. With  $t_s = 2.05$ , for  $T \in (t_s, t_c]$  we can define uniform exponential bounds with  $\sigma = 0.31$  and  $\nu = 3.29$ . Figure 6 shows the FTLEs  $\mu^\pm$ .

In the general case with linear-time-varying (LTV) tangent dynamics, there is similar behavior requiring the truncation of the time interval. The specification of the constants  $t_s$  and  $t_c$  can be exclusively based on behavior of the  $\mu^\pm$  and  $\mu_{EB}^\pm$ ; it is not necessary to determine angles within subspaces as was done in this example to provide insight into the root cause.

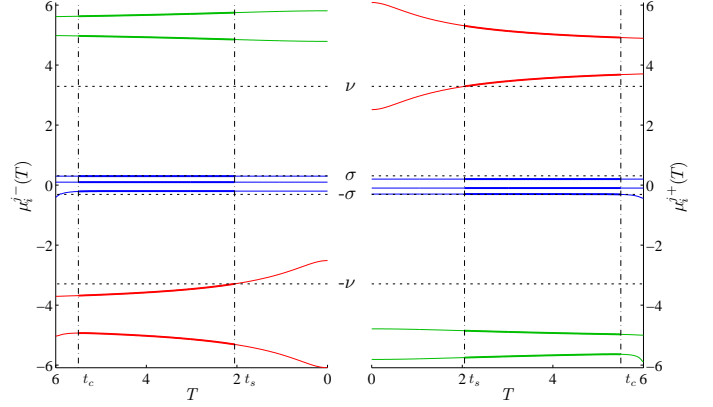


Figure 5: Backward and forward FTLEs ( $\mu_i^\pm$  with  $i = 1, \dots, n^j$  and  $j = s, c, u$ ) for the subspaces  $\mathcal{E}^s$  (green),  $\mathcal{E}^u$  (red) and  $\mathcal{E}^c$  (blue). The exponential bound constants  $\sigma$  and  $\nu$  and the start and cutoff times  $t_s$  and  $t_c$  are shown.

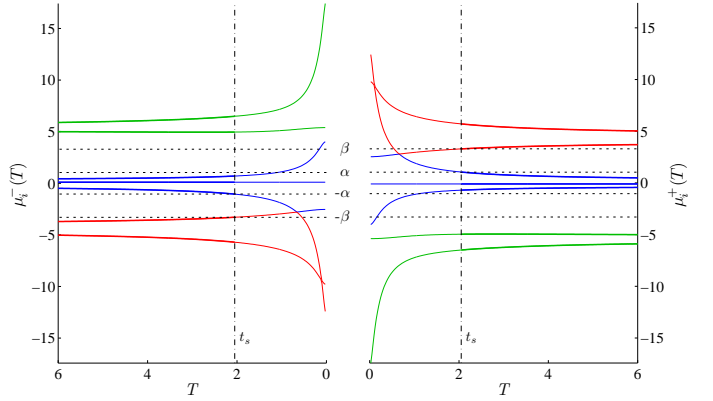


Figure 6: Backward and forward FTLEs ( $\mu_i^\pm$  with  $i = 1, \dots, n$ ). The constants  $\alpha$  and  $\beta$  and the start time  $t_s$  are shown.

## 7.2. Davis-Skodje 2D System: Attracting Slow Manifold

Davis and Skodje (D-S) [10] introduced a 2D nonlinear system

$$\begin{aligned}\dot{x}_1 &= -x_1, \\ \dot{x}_2 &= -\gamma x_2 + \frac{(\gamma-1)x_1 + \gamma x_1^2}{(1+x_1)^2}\end{aligned}\quad (33)$$

defined on the state space  $\{(x_1, x_2) \in \mathbb{R}^2 : x_1 \geq 0 \text{ and } x_2 \geq 0\}$  with constant  $\gamma > 1$ , which has become a benchmark for center manifold determination. The origin is a globally attracting equilibrium point, but more importantly in the present context, for sufficiently large  $\gamma$ , trajectories are first attracted on a faster timescale to the 1D center manifold

$$\mathcal{W}^c = \{(x_1, x_2) \in \mathbb{R}^2 : x_2 = x_1/(1+x_1)\}, \quad (34)$$

and then follow  $\mathcal{W}^c$  to the origin on a slower timescale. The two timescales are evident in the analytic solution

$$\phi(t; x_1, x_2) = \begin{bmatrix} x_1 e^{-t} \\ \left(x_2 - \frac{x_1}{1+x_1}\right) e^{-\gamma t} + \frac{x_1}{1+x_1} e^{-t} \end{bmatrix}. \quad (35)$$

for the flow associated with the vector field in (33). Note that if the initial state is on the center manifold, there is no fast

timescale behavior because the coefficient of  $e^{-\gamma t}$  in (35) is zero. For this system, both the nonlinear and tangent linear dynamics have two timescales, and it is appropriate to refer to the center manifold as the slow manifold.

The invariant center manifold  $\mathcal{W}^c$  and several other trajectories are shown in Fig. 7 for  $\gamma = 10$ . The time interval between dots on the trajectory is 0.1, illustrating faster motion off  $\mathcal{W}^c$  than on  $\mathcal{W}^c$ . From the analytical representation (34) for the center manifold, we know that for any  $\mathbf{x} \in \mathcal{W}^c$ ,

$$T_{\mathbf{x}}\mathcal{W}^c = \text{span}\{[(1+x_1)^2 \quad 1]^T\}. \quad (36)$$

The linearized dynamics (2) for the D-S system have the Jacobian matrix

$$D\mathbf{f} = \begin{bmatrix} -1 & 0 \\ \frac{(\gamma-1)+(\gamma+1)x_1}{(1+x_1)^3} & -\gamma \end{bmatrix}. \quad (37)$$

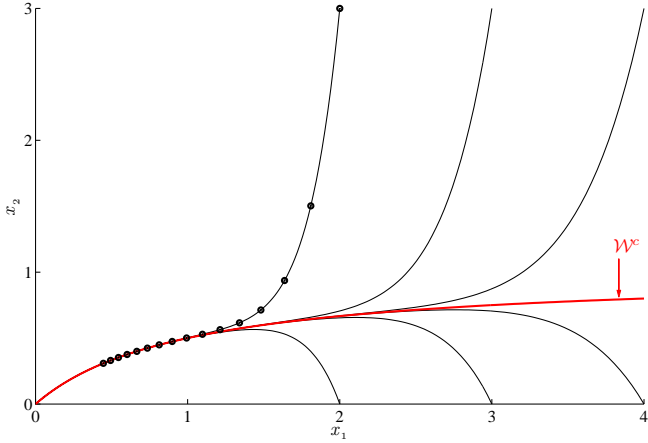


Figure 7: Sample trajectories of the D-S system for  $\gamma = 10.0$  with the center manifold  $\mathcal{W}^c$  indicated. The dots on the trajectory departing from  $\mathbf{x} = (3, 2)$  are computed with  $\Delta t = 0.1$  and illustrate faster motion off the center manifold than on.

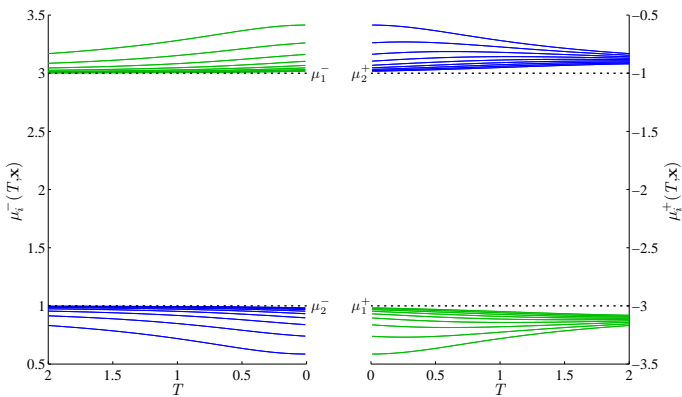


Figure 8: Superposition of forward and backward FTLEs for the Davis-Skodje system for various values of  $\mathbf{x}$  illustrating uniformity.

Given the presence of the equilibrium point, other approaches based on eigen-analysis at the equilibrium point are applicable: for example, integrating (33) backward from an initial state perturbed slightly from the origin in the direction of the eigenvector associated with the largest eigenvalue to compute

$\mathcal{W}^c$ . However our purpose here is to demonstrate the methodology developed in this paper, methodology that does not require the presence of an equilibrium point.

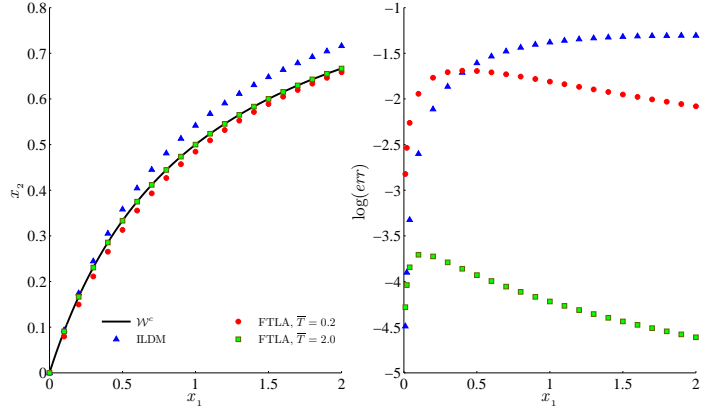


Figure 9: *Left plot*: Exact center invariant manifold  $\mathcal{W}^c$  and its approximations calculated via FTLA and ILDM methods for several values of  $x_1$ . FTLA results are shown for two different averaging times have been used:  $\bar{T} = 0.2$  and  $\bar{T} = 2.0$ . *Right plot*: ILDM and FTLA center manifold approximation errors.

### 7.2.1. Finite-Time Lyapunov Analysis

We now demonstrate the numerical application of FTLA for the case  $\gamma = 3$ , the case also investigated in [10]. We consider the set  $\mathcal{X} = \{(x_1, x_2) \in \mathbb{R}^2 : 0 \leq x_1 \leq 2.0 \text{ and } 0 \leq x_2 \leq 1.0\}$  and check if the system (33), with  $\gamma = 3.0$ , satisfies the conditions in Def. 5.1 for a finite-time uniform two-timescale set. Figure 8 shows the superposition of the forward and backward FTLEs, as functions of  $T$ , for a uniform grid of points in  $\mathcal{X}$ . The only possibility for two timescales is to consider  $n^s = 1$ ,  $n^c = 1$ ,  $n^u = 0$ . Then with  $\alpha = 1.0$ ,  $\beta = 3.0$ ,  $\Delta\mu = 2.0$ ,  $\sigma = 1.0$ ,  $\nu = 3.0$ ,  $t_s = 0$ ,  $t_c = \bar{T}$ , and  $\bar{T} \geq 2.0$ , the Def. 5.1 conditions are satisfied, and we conclude that  $\mathcal{X}$  is a uniform two-timescale set resolvable over at least 4 convergence time constants. For the D-S system, it can be verified that the timescale behavior is globally uniform, so that there is no upper limit on  $\bar{T}$  unless numerical errors are an issue. The FTLVs that approximate the fast and slow directions are  $\mathbf{l}_1^+(T, \mathbf{x})$  and  $\mathbf{l}_2^-(T, \mathbf{x})$ .

FTLA indicates the potential existence of a one-dimensional center manifold that can be parametrized by  $x_1$ . Candidate center manifold points, namely, points that satisfy the orthogonality condition  $\langle \mathbf{f}(\mathbf{x}), \mathbf{l}_1^-(\bar{T}, \mathbf{x}) \rangle = 0$  are shown in Fig. 9 with  $\bar{T} = 0.2$  and  $\bar{T} = 2.0$ . Over time intervals around  $t_f = 1$ , attraction to the center manifold occurs before the equilibrium point at the origin is reached. Because the slow and fast timescales are not very different for  $\gamma = 3.0$ , there is not as strong an attraction to the center manifold as would be the case for larger values of  $\gamma$ , yet even for this modest level of timescale separation, the two-timescale structure can be resolved.

### 7.2.2. Asymptotic Lyapunov Analysis

For the D-S system, because the timescale structure is uniform on the entire state space, the progress toward convergence in the first 2 units of time continues, and it is possible to compute the asymptotic Lyapunov exponents and vectors.

The infinite-time limits of the FTLEs can be determined analytically to be  $\mu_1^+ = -\gamma$ , and  $\mu_2^+ = -1$ . The backward time limits are  $(\mu_1^-, \mu_2^-) = (\gamma, 1) = (-\mu_1^+, -\mu_2^+)$ .

We can analytically compute the center FTLV  $\mathbf{I}_2^-(T, \mathbf{x})$  as the eigenvector of  $\Phi(-T, \mathbf{x})^T \Phi(-T, \mathbf{x})$  corresponding to  $\mu_2^-(T, \mathbf{x})$ , the center exponent in backward time. As  $T$  goes to infinity,  $\mathbf{I}_2^-(T, \mathbf{x})$  can be shown to converge to

$$\mathbf{I}_2^-(\mathbf{x}) = a(x_1, x_2) \begin{bmatrix} (1 + x_1)^2 \\ 1 \end{bmatrix} \quad (38)$$

where  $a(x_1, x_2)$  is a non-zero scalar function. For  $\mathbf{I}_2^-$  to be a unit vector,  $a(x_1, x_2)$  should be chosen appropriately. Similarly  $\mathbf{I}_1^+(T, \mathbf{x})$  can be shown to converge to

$$\mathbf{I}_1^+(\mathbf{x}) = \begin{bmatrix} 0 \\ 1 \end{bmatrix} \quad (39)$$

independent of  $\mathbf{x}$ .

If a point  $\mathbf{x}$  is on  $\mathcal{W}^c$ , then, using the asymptotic Lyapunov vector  $\mathbf{I}_1^+(\mathbf{x})$ , the orthogonality condition characterizing points on  $\mathcal{W}^c$  is in agreement with (34). These asymptotic results lend credence to the finite-time results, but the most important message is that in 2 units of time, the two-timescale behavior can be diagnosed and an accurate approximation of the center manifold can be obtained.

### 7.2.3. Invariant Center Manifold Approximation Using Eigenvectors of $\mathbf{Df}$

The eigenvalues of  $\mathbf{Df}$  in (37) are  $-\gamma$  and  $-1$ ; in this case they indicate the two-timescale behavior correctly. Assuming that the span of the eigenvector, denoted  $\mathbf{e}^c$ , associated with the center eigenvalue  $-1$ , approximates the center subspace of the tangent plane, the ILDM method [41] estimates points on  $\mathcal{W}^c$  by computing solutions to the orthogonality condition  $\langle \mathbf{f}(\mathbf{x}), (\mathbf{e}^c)^\perp \rangle = 0$ . The center eigenvector  $\mathbf{e}^c$  can be obtained analytically and is

$$\mathbf{e}^c = \begin{bmatrix} (1 + x_1)^3 \\ 1 + \frac{(\gamma+1)}{(\gamma-1)}x_1 \end{bmatrix}. \quad (40)$$

The ILDM approximation to the center manifold is

$$x_2 = \frac{x_1}{1 + x_1} + \frac{2x_1^2}{\gamma^2} \left[ \frac{1}{(1 - \frac{1}{\gamma})(1 + x_1)^3} \right]. \quad (41)$$

Figure 9 shows the exact manifold  $\mathcal{W}^c$  along with approximations calculated with the ILDM and FTLA methods. The ILDM approximation is accurate around the equilibrium point (small  $x_1$ ) but gets worse away from the origin. The error is proportional to  $\varepsilon^2$ , where  $\varepsilon = 1/\gamma$ , consistent with the analysis in [31]. The FTLA method provides uniformly accurate approximations when a sufficiently large averaging time is used.  $\bar{T} = 2.0$  is large enough here, whereas  $\bar{T} = 0.2$  is not. The center manifold approximation errors are calculated so that  $err = |x_2^{\mathcal{W}^c} - \hat{x}_2|$  where  $x_2^{\mathcal{W}^c}$  is the exact  $x_2$ -coordinate defined in (34) and  $\hat{x}_2$  represents the ILDM or FTLA  $x_2$ -coordinate approximation.

### 7.3. 3D Nonlinear System: Normally Hyperbolic Center Manifold

Consider a nonlinear time-invariant system

$$\begin{aligned} \dot{x}_1 &= ax_1, \\ \dot{x}_2 &= bx_2 + \gamma(b - 2a)x_1^2, \\ \dot{x}_3 &= cx_3 + \gamma(c - 2a)x_1^2. \end{aligned} \quad (42)$$

For the numerical results, the constants are assigned the values  $a = -0.2$ ,  $b = -3$ ,  $c = 3$ , and  $\gamma = 2$ .

#### 7.3.1. Finite-Time Lyapunov Analysis

First the FTLEs are computed on a uniform grid on the cubic region  $\mathcal{X} = [-10, 10]^3 \subset \mathbb{R}^3$ . Figure 10 shows a superposition of all the forward and backward FTLEs as functions of averaging time for the 36 values of  $\mathbf{x}$  on the  $\mathcal{X}$  grid. The only possibility for two timescales is  $n^s = n^c = n^u = 1$ . With  $\alpha = 0.8$ ,  $\beta = 3.0$ ,  $\Delta\mu = 2.2$ ,  $\sigma = 0.5$ ,  $\nu = 3.0$ ,  $t_s = 0$ ,  $t_c = \bar{T}$  and  $\bar{T} = 3.0$ , the Def. 5.1 requirements for a uniform two-timescale set resolvable over 6.64 convergence time constants are satisfied.

Having diagnosed two timescales and both fast-stable and fast-unstable behavior, there may be a 1D center manifold and, if so, it is normally hyperbolic. Because there is sufficient averaging time,  $[\mathcal{E}^c(\bar{T}, \mathbf{x})]^\perp = \text{span}\{\mathbf{I}_1^-(\bar{T}, \mathbf{x}), \mathbf{I}_3^+(\bar{T}, \mathbf{x})\}$ , the application of the general result (26), is a good approximation of the orthogonal complement to the corresponding invariant center subspace, and an accurate approximation to invariant center manifold can be obtained.

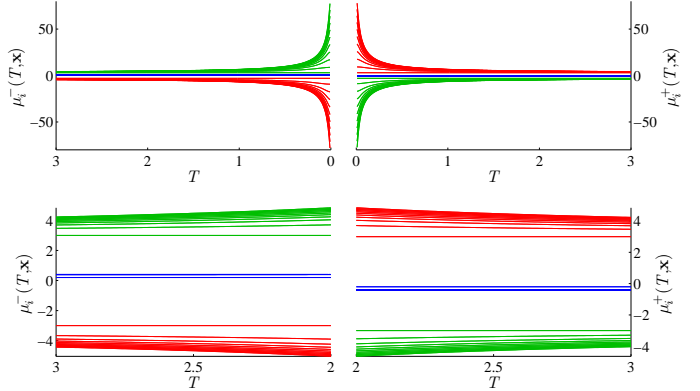


Figure 10: Forward and backward finite-time Lyapunov exponents for grid points on  $\mathcal{X}$ . For forward time,  $\mu_1^+(T, x)$ ,  $\mu_2^+(T, x)$ ,  $\mu_3^+(T, x)$  are green, blue, red, resp. For backward time,  $\mu_3^-(T, x)$ ,  $\mu_2^-(T, x)$ ,  $\mu_1^-(T, x)$  are red, blue, green, resp. The two lower plots zoom in on the final interval of  $T$ .

After examining the FTLVs, we chose  $x_1$  to parametrize  $\mathcal{W}^c$ , because its coordinate axis is not parallel to any of the directions in  $[\mathcal{E}^c(\bar{T}, \mathbf{x})]^\perp$ . For each of the values on the grid over  $x_1$ , we compute the values of  $x_2$  and  $x_3$  that satisfy the orthogonality conditions. The resulting finite-time approximation of the postulated invariant center manifold for values of  $x_1$  from -10 to 10 is plotted in Fig. 11.

#### 7.3.2. Invariant Center Manifold

For this problem, there is an invariant center manifold and a means of determining it, allowing the accuracy of FTLA to be



assessed. Over a time interval long relative to the fast timescale, yet short relative to the slow timescale, trajectories approach the 2D manifolds  $\mathcal{W}^{cu}$  and  $\mathcal{W}^{cs}$ , in forward and backward time respectively, given by

$$\begin{aligned}\mathcal{W}^{cu} &= \{(x_1, x_2, x_3) \in \mathbb{R}^3 \mid x_2 + \gamma x_1^2 = 0\}, \\ \mathcal{W}^{cs} &= \{(x_1, x_2, x_3) \in \mathbb{R}^3 \mid x_3 + \gamma x_1^2 = 0\}.\end{aligned}\quad (43)$$

The intersection of these sets is the invariant center manifold:  $\mathcal{W}^c = \mathcal{W}^{cu} \cap \mathcal{W}^{cs}$ . These manifolds and their intersection are shown in Fig. 11.

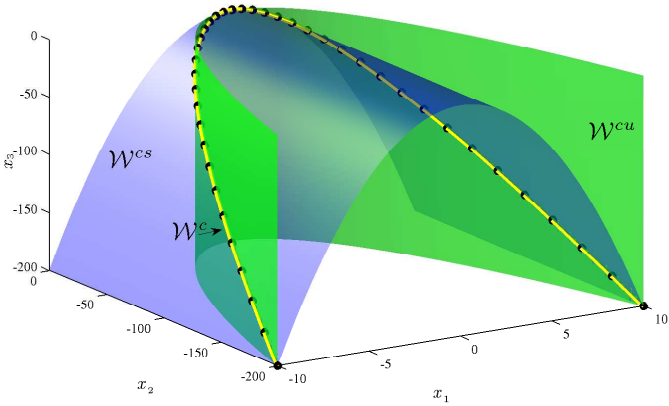


Figure 11: Invariant center manifold  $\mathcal{W}^c$  (yellow curve) as the intersection of the 2D manifolds  $\mathcal{W}^{cu}$  (green surface) and  $\mathcal{W}^{cs}$  (purple surface). The black rings and dots represent the FTLA approximations of points on the invariant center manifold calculated for  $\bar{T} = 3.0$ .

At a point  $\mathbf{x} \in \mathcal{W}^c$ , the vectors normal to  $\mathcal{W}^{cu}$  and  $\mathcal{W}^{cs}$  are given by  $\eta_1(\mathbf{x}) = [2\gamma x_1 \ 1 \ 0]^T$  and  $\eta_2(\mathbf{x}) = [2\gamma x_1 \ 0 \ 1]^T$  respectively. Points on  $\mathcal{W}^c$ , due to its invariance with respect to the flow, satisfy the orthogonality conditions

$$\begin{aligned}0 &= \langle \eta_1(\mathbf{x}), \mathbf{f}(\mathbf{x}) \rangle = \langle [2\gamma x_1 \ 1 \ 0]^T, \mathbf{f}(\mathbf{x}) \rangle \\ &= 2\gamma a x_1^2 + b x_2 + \gamma(b - 2a)x_1^2 = b(x_2 + \gamma x_1^2) \\ 0 &= \langle \eta_2(\mathbf{x}), \mathbf{f}(\mathbf{x}) \rangle = \langle [2\gamma x_1 \ 0 \ 1]^T, \mathbf{f}(\mathbf{x}) \rangle \\ &= 2\gamma a x_1^2 + c x_3 + \gamma(c - 2a)x_1^2 = c(x_3 + \gamma x_1^2)\end{aligned}\quad (44)$$

where  $\mathbf{f}(\mathbf{x})$  is the vector field given in (42). Figure 12 shows  $\alpha^+(T, \mathbf{x})$  and  $\alpha^-(T, \mathbf{x})$  which are respectively the angles between  $\mathbf{I}_3^+(T, \mathbf{x})$  and  $\eta_2(\mathbf{x})$  and between  $\mathbf{I}_1^-(T, \mathbf{x})$  and  $\eta_1(\mathbf{x})$ . The angles are functions of  $T$  and are plotted for several values of  $x_1$ . As the averaging time increases, the FTLVs used to approximate the directions of the normal vectors to the invariant center manifold align with those vectors.

For a given  $x_1$ , letting  $(x_1, \hat{x}_2, \hat{x}_3)$  denote an approximation of the invariant center manifold point  $(x_1, -\gamma x_1^2, -\gamma x_1^2)$ , we define the approximation error to be  $err = [(\hat{x}_2 + \gamma x_1^2)^2 + (\hat{x}_3 + \gamma x_1^2)^2]^{1/2}$ . The approximation errors for FTLA are calculated using  $\bar{T} = 1.0$ ,  $\bar{T} = 2.0$  and  $\bar{T} = 3.0$  and plotted in Fig. 13.

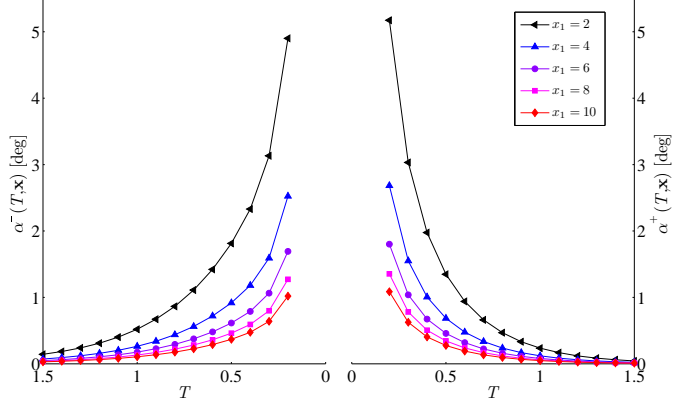


Figure 12: Angles between  $\mathbf{I}_1^-(T, \mathbf{x})$ ,  $\mathbf{I}_3^+(T, \mathbf{x})$  and the directions normal to the invariant center manifold  $\eta_1(\mathbf{x})$ ,  $\eta_2(\mathbf{x})$  versus the averaging time  $T$ . Points are plotted for different values of  $x_1$ .

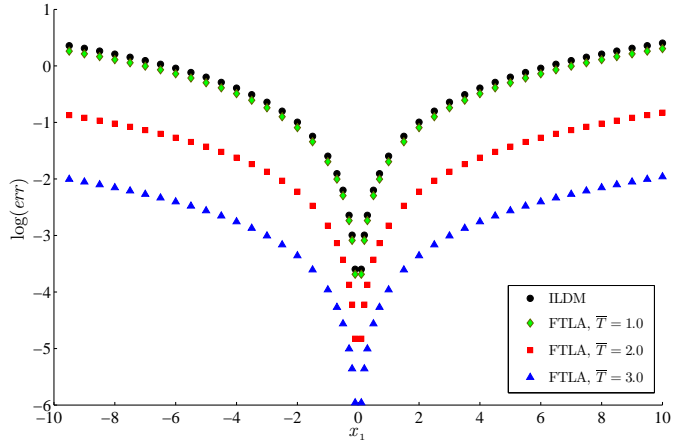


Figure 13: ILDM and FTLA center manifold approximation errors calculated for various values of the independent variable  $x_1$ . The FTLA approximation errors are provided for averaging times  $\bar{T} = 1.0, 2.0, 3.0$ .

### 7.3.3. Invariant Center Manifold Approximation Using Eigenvectors of $D\mathbf{f}(\mathbf{x})$

Using the eigenvalues and eigenvectors of  $D\mathbf{f}(\mathbf{x})$  (the ILDM method [41]), it is assumed that the eigenvector corresponding to the center eigenvalue spans the center subspace. The Jacobian matrix corresponding to the system (42) is

$$D\mathbf{f} = \begin{bmatrix} a & 0 & 0 \\ 2\gamma(b - 2a)x_1 & b & 0 \\ 2\gamma(c - 2a)x_1 & 0 & c \end{bmatrix}\quad (45)$$

and the eigenvector corresponding to the center eigenvalue,  $\lambda_c = a$  for the numerical values used, can be written as

$$\mathbf{v}_c = \left[ 1, \quad -2\gamma x_1 \left( \frac{b-2a}{b-a} \right), \quad -2\gamma x_1 \left( \frac{c-2a}{c-a} \right) \right]^T \quad (46)$$

Two linearly independent vectors orthogonal to  $\mathbf{v}_c$  are

$$\mathbf{w}_1 = \left[ 2\gamma x_1 \left( \frac{b-2a}{b-a} \right), \quad 1, \quad 0 \right]^T, \quad \mathbf{w}_2 = \left[ 2\gamma x_1 \left( \frac{c-2a}{c-a} \right), \quad 0, \quad 1 \right]^T \quad (47)$$

Points on the invariant center manifold are approximated using solutions to the orthogonality conditions

$$\langle \mathbf{w}_1, \mathbf{f}(\mathbf{x}) \rangle = 0, \quad \langle \mathbf{w}_2, \mathbf{f}(\mathbf{x}) \rangle = 0 \quad (48)$$

For given  $x_1$ , the magnitudes of the errors in  $x_2$  and  $x_3$  relative to the correct values for  $\mathcal{W}^c$  are  $2\gamma x_1^2 \frac{a^2}{(a-b)b}$  and  $2\gamma x_1^2 \frac{a^2}{(a-c)c}$  respectively. Taking the norm of these errors, the center manifold approximation error for the ILDM method is plotted in Fig. 13. The ILDM error is similar to that for FTLA when the averaging time is  $\bar{T} = 1.0$ , but FTLA gives greater accuracy for the longer averaging times  $\bar{T} = 2.0$  and  $\bar{T} = 3.0$ .

#### 7.4. 4D Hamiltonian System: Mass-Spring-Damper System

To demonstrate the use of FTLA to locate points on a two-dimensional normally hyperbolic center manifold, we consider the optimal control of a mass-(nonlinear) spring-damper system modeled as

$$\begin{aligned}\dot{x}_1 &= x_2, \\ \dot{x}_2 &= -\frac{1}{m} \left( cx_2 + k_1 x_1 + k_2 x_1^3 \right) + \frac{u}{m},\end{aligned}\quad (49)$$

where  $x_1$  is the displacement of the mass  $m$  measured from the rest position of the spring,  $u$  is the applied scalar control,  $k_1$  and  $k_2$  are the coefficients of the linear and cubic contributions to the spring force, and  $c$  is the damping coefficient. For the problem of minimizing the function

$$\min J = \int_0^{t_f} \frac{1}{2} u^2 dt, \quad (50)$$

subject to the dynamic constraint (49) and specified initial and final conditions on  $x_1$  at a specified final time  $t_f$ , Pontryagin's minimum principle leads to first-order necessary conditions in the form of a boundary value problem for the Hamiltonian system

$$\begin{aligned}\dot{x}_1 &= x_2, \\ \dot{x}_2 &= -\frac{1}{m} \left( cx_2 + k_1 x_1 + k_2 x_1^3 + \frac{\lambda_2}{m} \right), \\ \dot{\lambda}_1 &= \frac{\lambda_2}{m} \left( k_1 + 3k_2 x_1^2 \right), \\ \dot{\lambda}_2 &= -\lambda_1 + c \frac{\lambda_2}{m},\end{aligned}\quad (51)$$

where  $\lambda_1$  and  $\lambda_2$  are adjoint variables and the minimizing control is  $u^* = -\lambda_2/m$ . For consistency with the rest of the paper, we consider (51) in the form  $\dot{\mathbf{x}} = \mathbf{f}(\mathbf{x})$  with  $\mathbf{x} = [x_1, x_2, \lambda_1, \lambda_2]^T \in \mathbb{R}^4$  and  $\mathbf{f}$  defined appropriately.

For small values of  $m$ , the Hamiltonian system is in singularly perturbed standard form [33], and the system can be expected to evolve on disparate timescales. Using the two-timescale geometry to solve the boundary-value problem has been addressed in [4, 23, 49, 58]. Here we focus on applying FTLA to the Hamiltonian system (51) to diagnose two-timescale behavior and locate points on the center manifold, which is in this case a slow manifold. The linearized dynamics (2) have the Jacobian matrix

$$D\mathbf{f} = \begin{bmatrix} 0 & 1 & 0 & 0 \\ \frac{1}{m}(-k_1 - 3k_2 x_1^2) & -\frac{c}{m} & 0 & -\left(\frac{1}{m}\right)^2 \\ \frac{\lambda_2}{m}(6k_2 x_1) & 0 & 0 & \frac{1}{m}(k_1 + 3k_2 x_1^2) \\ 0 & 0 & -1 & \frac{c}{m} \end{bmatrix}. \quad (52)$$

For the numerical results we use  $m = 0.5$ ,  $k_1 = 1$ ,  $k_2 = 0.01$ , and  $c = 4\sqrt{k_1 m}$ .

##### 7.4.1. Finite-Time Lyapunov Analysis

FTLA is applied in a region  $\mathcal{X} = (-1.0, 6.0) \times (-5.0, -1.9) \times (7.0, 15.0) \times (0.8, 5.0)$ , chosen such that the ILDM method is applicable (i.e., the eigenvalues of  $D\mathbf{f}$  are real), yet the center manifold curvature is large enough that the ILDM method produces noticeable errors. We present results for the five points:  $\mathbf{x}_1 = [3.00, -2.0, 7.5, 2.0]^T$ ,  $\mathbf{x}_2 = [2.85, -2.0, 9.3, 2.0]^T$ ,  $\mathbf{x}_3 = [2.70, -2.0, 11.0, 2.0]^T$ ,  $\mathbf{x}_4 = [2.55, -2.0, 12.8, 2.0]^T$ , and  $\mathbf{x}_5 = [2.40, -2.0, 14.5, 2.0]^T$ , that are representative of all the points in  $\mathcal{X}$ . Figure 14 shows the forward and backward Lyapunov exponents for the five points as functions of the averaging time  $T$ . Because the system is Hamiltonian, the FTLEs should be symmetric about the origin. With  $n^s = n^u = 1$ ,  $n^c = 2$ ,  $\alpha = 0.52$ ,  $\beta = 5.64$ ,  $\Delta\mu = 5.12$ ,  $\sigma = 0.66$ ,  $\nu = 5.19$ ,  $t_s = 0$  and  $t_c = \bar{T} = 0.50$ , the conditions given in Def. 5.1 for a uniform two-timescale set resolvable over 2.6 convergence time constants are satisfied. Figure 15 shows the FTLEs and exponential bounds that were computed as described in Section 6.1.

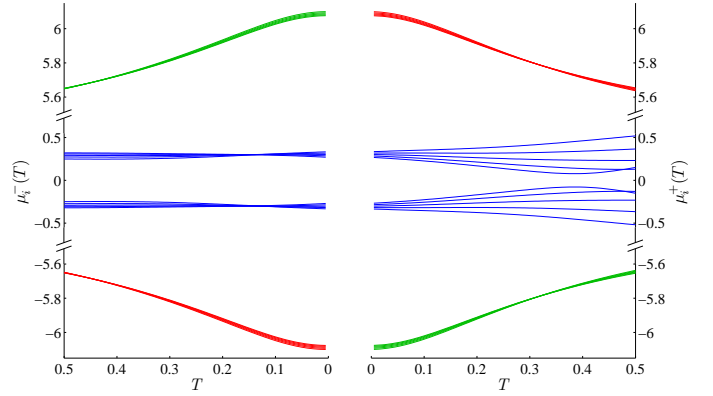


Figure 14: Superposition of backward and forward FTLEs for points  $\mathbf{x}_1, \mathbf{x}_2, \mathbf{x}_3, \mathbf{x}_4$ , and  $\mathbf{x}_5$ . Note that only segments of the y-axis are shown to highlight the center FTLEs.

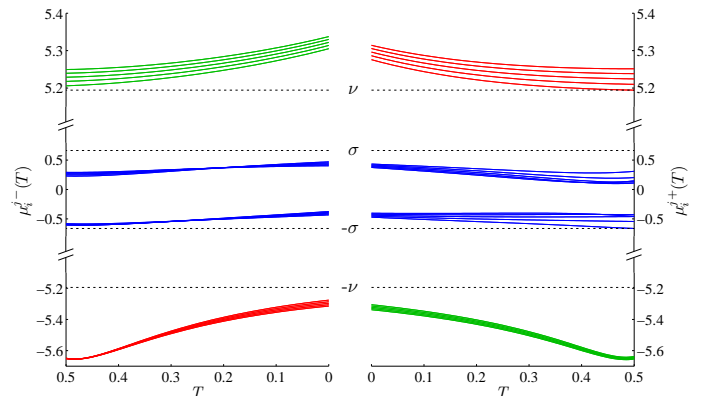


Figure 15: FTLEs  $\mu_i^j$  with  $i = 1, \dots, n^j$  and  $j = s, c, u$  for the subspaces  $\mathcal{E}^s(0.5, \mathbf{x})$ ,  $\mathcal{E}^c(0.5, \mathbf{x})$ ,  $\mathcal{E}^u(0.5, \mathbf{x})$  and determination of the constants  $\nu$  and  $\sigma$  for  $\mathbf{x}_1, \mathbf{x}_2, \mathbf{x}_3, \mathbf{x}_4$ , and  $\mathbf{x}_5$  as functions of time. The distance between  $\nu$  and  $\sigma$  is actually larger than it appears since only segments of the vertical axis are shown.

#### 7.4.2. Computing Center Manifold Points Using FTLA

The center subspace  $\mathcal{E}^c(\bar{T}, \mathbf{x})$  has dimension  $n^c = 2$  and can be written as (see (17))

$$\mathcal{E}^c(\bar{T}, \mathbf{x}) = \mathcal{L}_3^+(\bar{T}, \mathbf{x}) \cap \mathcal{L}_2^-(\bar{T}, \mathbf{x}) \quad (53)$$

with its orthogonal complement (26) given by

$$[\mathcal{E}^c(\bar{T}, \mathbf{x})]^\perp = \text{span}\{\mathbf{I}_1^-(\bar{T}, \mathbf{x}), \mathbf{I}_4^+(\bar{T}, \mathbf{x})\}. \quad (54)$$

The existence of a 2D center manifold is postulated. As described in Section 5,  $n^c$  coordinates are chosen to parametrize  $\mathcal{W}^c$  such that their coordinates axes are not parallel to any of the directions in  $[\mathcal{E}^c(\bar{T}, \mathbf{x})]^\perp$ , namely in  $\mathbf{I}_1^-(\bar{T}, \mathbf{x})$  and  $\mathbf{I}_4^+(\bar{T}, \mathbf{x})$  directions. For example

$$\begin{aligned} \mathbf{I}_1^-(0.5, \mathbf{x}_1) &= [0.33, 0.89, 0.05, 0.31]^T, \\ \mathbf{I}_4^+(0.5, \mathbf{x}_1) &= [-0.01, 0.00, -0.16, 0.99]^T. \end{aligned} \quad (55)$$

The directions of  $x_2$  and  $\lambda_2$  are almost parallel respectively to  $\mathbf{I}_1^-$  and  $\mathbf{I}_4^+$ , so we choose the independent variables to be  $x_1$  and  $\lambda_1$ . We use the  $(x_1, \lambda_1)$  coordinates of the five points  $\mathbf{x}_j$ ,  $j = 1, \dots, 5$  as the grid in the independent coordinate plane and compute the  $(x_2, \lambda_2)$  coordinates for the graph of  $\mathcal{W}^c(T)$  by solving the orthogonality conditions.

For Def. 5.1, the value of  $\bar{T}$  must apply at each point in  $\mathcal{X}$ ; to do so, it must be the minimum over all the maximum forward and backward averaging times on  $\mathcal{X}$ . It can be beneficial in computing center manifold points to use averaging times greater than  $\bar{T}$  when possible. An iterative procedure for determining the averaging time during convergence toward the center manifold is described in Appendix B. For the converged points, the forward and backward averaging times were increased to 5.0 and 2.0 respectively.

Because the exact location of the invariant center manifold is not known, we use the following means to assess accuracy. The estimated invariant center manifold points  $\hat{\mathbf{x}}_j$ ,  $j = 1, \dots, 5$  are propagated backward and forward in time to  $\phi(t^\pm, \hat{\mathbf{x}}_j)$ . Then for each of the end points, we fix the independent variables,  $x_1$  and  $\lambda_1$ , and use FTLA to recompute the dependent variables,  $x_2$  and  $\lambda_2$  for the center manifold point estimate. If the FTLA method computed points on the invariant center manifold without error, then the propagated estimates and re-estimated points would be the same; the degree of inconsistency is thus an indication of accuracy and invariance. The same procedure is performed for the ILDM estimates.

Figure 16, showing points and trajectories projected onto the  $\lambda_1$ - $x_2$  plane, indicates that FTLA is much more consistent than the ILDM method. The trajectories departing from initial points calculated with FTLA (black circles) propagate to points (black squares forward and black diamonds backward) close to those re-estimated, the interpretation being that by starting closer to the invariant center manifold the trajectories follow the center manifold for a longer time. Although the initial ILDM points (red circles) appear close to the initial FTLA points, the high degree of inconsistency at the end points indicates greater inaccuracy.

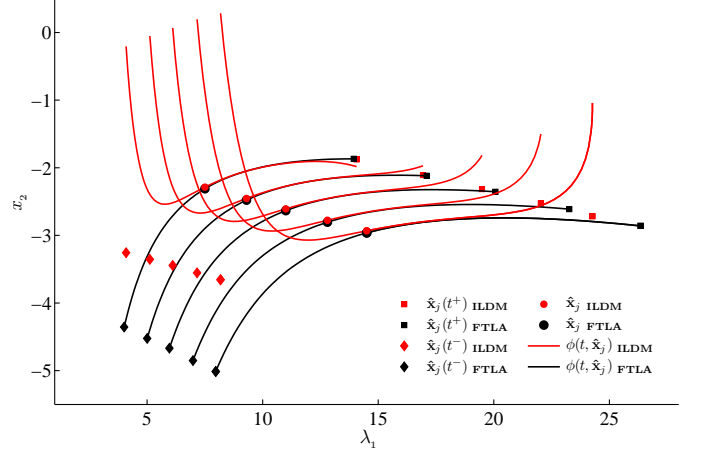


Figure 16: Projection onto the  $\lambda_1$ - $x_2$  plane of the forward and backward propagations from initial points on the center manifold (circles). The independent coordinates of the points at the end of the trajectories are used to compute new estimates on the center manifold (diamonds-backward, squares-forward). Points in black refer to estimates calculated via FTLA while the lighter ones are computed with ILDM.

Table 1: Invariance error percent for  $x_2$  and  $\lambda_2$  for FTLA and ILDM methods.

	$IP_{x_2}^+$		$IP_{x_2}^-$		$IP_{\lambda_2}^+$		$IP_{\lambda_2}^-$	
	FTLA	ILDM	FTLA	ILDM	FTLA	ILDM	FTLA	ILDM
$\hat{\mathbf{x}}_1$	1E-4	5.7E0	5.1E-2	9.4E1	3.0E-4	1.1E1	6.0E-4	5.0E-1
$\hat{\mathbf{x}}_2$	3.0E-4	6.5E0	2.5E-2	9.8E1	5.0E-4	1.2E1	3.0E-4	5.6E-1
$\hat{\mathbf{x}}_3$	1.0E-4	2.2E1	2.0E-3	1.0E2	2E-4	3.8E1	<1E-5	6.0E-1
$\hat{\mathbf{x}}_4$	2.8E-3	4.1E1	3.5E-2	1.1E2	4.6E-3	6.9E1	4.0E-4	6.5E-1
$\hat{\mathbf{x}}_5$	1.4E-2	6.2E1	8.0E-2	1.1E2	2.2E-2	1.0E2	1.0E-4	6.9E-1

Table 1 shows quantitatively the center manifold estimation error for the FTLA and ILDM methods. An invariance error percent (IP) is defined by

$$IP_{x_2}^\pm = \frac{\|x_2(\hat{\mathbf{x}}_j(t^\pm)) - x_2(\phi(t^\pm, \hat{\mathbf{x}}_j))\|}{\|x_2(\hat{\mathbf{x}}_j(t^\pm))\|} * 100 \quad (56)$$

where  $\hat{\mathbf{x}}_j(t^+)$  (squares) and  $\hat{\mathbf{x}}_j(t^-)$  (diamonds) are estimates of points on the center manifold calculated respectively from  $\phi(t^+, \hat{\mathbf{x}}_j)$  and  $\phi(t^-, \hat{\mathbf{x}}_j)$  via FTLA or ILDM. The trajectory end points  $\phi(t^\pm, \hat{\mathbf{x}}_j)$  in Fig. 16) are for  $t^+ = 1.5$  and  $t^- = -1.0$ . Finally  $x_2(\cdot)$  denotes the  $x_2$  coordinate of argument. The explanation for  $IP_{\lambda_2}^\pm$  is analogous. The IP values indicate that FTLA produces accurate approximations to points on the invariant center manifold and is significantly more accurate than the ILDM method.

## 8. Conclusions

The practical goal of this work was to use finite-time Lyapunov analysis to improve accuracy, and extend applicability, relative to the intrinsic low-dimensional manifold method, in estimating points on slow manifolds and more generally normally hyperbolic center manifolds. This has been accom-

plished as demonstrated in several examples of increasing dimension and complexity. In addition, a definition of a uniform finite-time two-timescale set has been proposed with requirements on the finite-time Lyapunov spectrum and the subspaces constructed from the finite-time Lyapunov vectors, accounting for finite-time features - non-modal growth and rate of subspace convergence to the desired invariant subspaces. Although the examples show there exist systems for which the finite-time Lyapunov analysis method is viable, further experience is needed to clarify how broadly applicable it is.

Finite-time Lyapunov analysis of the tangent linear dynamics provides an alternative diagnostic approach to eigen-analysis of the associated system matrix (the Jacobian matrix associated with the vector field). Though we have used this finite-time information for approximating points on invariant manifolds, the finite-time information could potentially be used (a) to suggest a transformation of coordinates leading to the standard form required for the analytical singular perturbation approach, or more generally to coordinates adapted to the manifold structure, (b) to guide the selection of independent and dependent variables in the application of the quasi-steady-state approximation, the zero-derivative approach, and the Roussel-Fraser partial differential equation approach, and (c) to obtain an invariant manifold approximation that could subsequently be refined by another method. Also in the solution of boundary-value problems for two-timescale systems, determining points on manifolds to approximate certain missing boundary conditions at each end is exactly what is needed.

## Acknowledgments

Stimulating discussions with S.-H. Lam started the first author on this research. Discussions with L.-S. Young and A. Gorodetski were instrumental for understanding the relevant dynamical systems theory. Helpful discussions with Y. B. Pesin and B. Villac are also acknowledged.

## Appendix A. Subspace Convergence

Proposition Appendix A.3 below gives the exponential rate at which the finite-time Lyapunov subspaces, introduced in Section 4.1 and expressed in terms of the FTLVs, evolve with increasing  $T$  toward their asymptotic limits, under hypotheses in which these limits exist. Most of the ideas in Proposition Appendix A.3 and its proof can be found in [14, 19]. The new element here is that convergence of a particular Lyapunov subspace is addressed explicitly, rather than the convergence of individual Lyapunov vectors (see [25] for an alternative approach for a special case of a co-dimension one subspace).

**Definition Appendix A.1.** [19] *The Lyapunov spectrum is strongly non-degenerate at a point  $\mathbf{x}$ , if there exists positive constants  $t_s$  and  $\delta$  such that the spectral gap between each neighboring pair of forward FTLEs,  $\mu_{i+1}^+(T, \mathbf{x}) - \mu_i^+(T, \mathbf{x})$ ,  $i = 1, \dots, n-1$ , is greater than  $\delta$  for all  $T > t_s$  and likewise for the backward exponents.*

To consider the convergence of a Lyapunov subspace  $\mathcal{L}_j^+(T, \mathbf{x})$  with  $T$ , we focus on a particular spectral gap and bound it for use in the proposition that follows.

**Definition Appendix A.2.** [Spectral Gap Lower Bound] *For a specified  $t_s > 0$ , the lower bound on the spectral gap  $\Delta\mu_j^+(\mathbf{x})$  between neighboring forward FTLEs  $\mu_j^+(T, \mathbf{x})$  and  $\mu_{j+1}^+(T, \mathbf{x})$ , for a particular  $j \in \{1, 2, \dots, n-1\}$ , is*

$$\Delta\mu_j^+(\mathbf{x}) := \inf_{T \geq t_s} (\mu_{j+1}^+(T, \mathbf{x}) - \mu_j^+(T, \mathbf{x})). \quad (\text{A.1})$$

Similarly the spectral gap bound  $\Delta\mu_k^-(\mathbf{x})$  between neighboring backward FTLEs  $\mu_{k-1}^-(T, \mathbf{x})$  and  $\mu_k^-(T, \mathbf{x})$  is defined as

$$\Delta\mu_k^-(\mathbf{x}) := \inf_{T > t_s} (\mu_{k-1}^-(T, \mathbf{x}) - \mu_k^-(T, \mathbf{x})). \quad (\text{A.2})$$

**Proposition Appendix A.3.** *Consider the dynamical system (1) on a compact invariant subset  $\mathcal{Y}$  of the state space  $\mathbb{R}^n$ . At a Lyapunov regular point  $\mathbf{x} \in \mathcal{Y}$  for which there exists  $t_s > 0$  and  $\delta > 0$  such that the Lyapunov spectrum is strongly non-degenerate for  $T > t_s$  and for which there is a nonzero lower bound  $\Delta\mu_j^+(\mathbf{x})$  on the spectral gap for a specific value of  $j$ , the subspace  $\mathcal{L}_j^+(T, \mathbf{x})$  approaches the fixed subspace  $\mathcal{L}_j^+(\mathbf{x})$ , defined in Section 4.2 in terms of the asymptotic Lyapunov exponent  $\mu_j^+(\mathbf{x})$ . It approaches at an exponential rate characterized, for every sufficiently small  $\Delta T > 0$ , by*

$$\text{dist}(\mathcal{L}_j^+(T, \mathbf{x}), \mathcal{L}_j^+(T + \Delta T, \mathbf{x})) \leq K e^{-\Delta\mu_j^+(\mathbf{x}) \cdot T}, \quad (\text{A.3})$$

for all  $T > t_s$ , where  $K > 0$  is  $\Delta T$  dependent but  $T$  independent. Similarly, as  $T$  increases, the subspace  $\mathcal{L}_k^-(T, \mathbf{x})$  approaches the fixed subspace  $\mathcal{L}_k^-(\mathbf{x})$  at a rate proportional to  $\exp(-\Delta\mu_k^-(\mathbf{x}) \cdot T)$ .

*Proof of Proposition Appendix A.3:* Using (13) we have

$$\begin{aligned} \text{dist}(\mathcal{L}_j^+(T, \mathbf{x}), \mathcal{L}_j^+(T + \Delta T, \mathbf{x})) &= \|L_j^+(T, \mathbf{x})^T L_j^+(T + \Delta T, \mathbf{x})\|_2 \\ &= \left\| \begin{bmatrix} \mathbf{l}_1^+(T, \mathbf{x})^T \\ \mathbf{l}_2^+(T, \mathbf{x})^T \\ \vdots \\ \mathbf{l}_j^+(T, \mathbf{x})^T \end{bmatrix} \begin{bmatrix} \mathbf{l}_{j+1}^+(T + \Delta T, \mathbf{x}) & \cdots & \mathbf{l}_n^+(T + \Delta T, \mathbf{x}) \end{bmatrix} \right\|_2 \\ &= \left\| \begin{bmatrix} \langle \mathbf{l}_1^+(T, \mathbf{x}), \mathbf{l}_{j+1}^+(T + \Delta T, \mathbf{x}) \rangle & \cdots & \langle \mathbf{l}_1^+(T, \mathbf{x}), \mathbf{l}_n^+(T + \Delta T, \mathbf{x}) \rangle \\ \vdots & & \vdots \\ \langle \mathbf{l}_j^+(T, \mathbf{x}), \mathbf{l}_{j+1}^+(T + \Delta T, \mathbf{x}) \rangle & \cdots & \langle \mathbf{l}_j^+(T, \mathbf{x}), \mathbf{l}_n^+(T + \Delta T, \mathbf{x}) \rangle \end{bmatrix} \right\|_2 \end{aligned} \quad (\text{A.4})$$

Using a result from [19], we have for  $T > 0$  to 1<sup>st</sup>-order in the time increment  $\Delta T$

$$\mathbf{l}_m^+(T + \Delta T) = (1 + c\Delta T)\mathbf{l}_m^+(T) + \Delta T \sum_{i=1(i \neq m)}^n \frac{[(\mathbf{n}_i^+)^T (A^T + A)\mathbf{n}_m^+]}{e^{(\mu_m^+ - \mu_i^+)T} - e^{(\mu_i^+ - \mu_m^+)T}} \mathbf{l}_i^+, \quad (\text{A.5})$$

where  $A = D\mathbf{f}(\mathbf{x})$  is the system matrix of the linearized dynamics (2),  $\mathbf{n}_i^+$  is a vector from the SVD of the transition matrix  $\Phi(T, \mathbf{x})$  as defined in Section 4.1,  $c$  is a constant that is inconsequential in the following developments and is thus left unspecified, the  $\mathbf{x}$  dependence has been suppressed, and all exponents

and vectors in the summation on the right-hand-side are evaluated at  $(T, \mathbf{x})$ . It follows that the inner products in (A.4) are

$$\langle \mathbf{I}_k^+(T, \mathbf{x}), \mathbf{I}_m^+(T + \Delta T, \mathbf{x}) \rangle = \Delta T \frac{[(\mathbf{n}_k^+)^T (A^T + A) \mathbf{n}_m^+]}{e^{(\mu_m^+ - \mu_k^+)T} - e^{(\mu_k^+ - \mu_m^+)T}}. \quad (\text{A.6})$$

Because  $k \in \{1, \dots, j\}$  and  $m \in \{j+1, \dots, n\}$ , we have  $\exp[(\mu_k^+(T, \mathbf{x}) - \mu_m^+(T, \mathbf{x}))T] \leq \exp[-\Delta\mu_j^+(\mathbf{x})T]$ . Let  $\bar{a} = \max_{\mathbf{x} \in \mathcal{Y}} \max_{i \in \{1, 2, \dots, n\}} |\lambda_i(A^T + A)|$ , the maximum eigenvalue magnitude of  $A^T + A$  over the set  $\mathcal{Y}$ . And let  $\alpha = \exp(-2\Delta\mu_j^+(\mathbf{x})T_1)$  for some  $T_1 > t_s$ . Then for  $T \geq T_1 > 0$  we have

$$|\langle \mathbf{I}_k^+(T, \mathbf{x}), \mathbf{I}_m^+(T + \Delta T, \mathbf{x}) \rangle| \leq \frac{\bar{a}\Delta T}{1 - \alpha} e^{-\Delta\mu_j^+(\mathbf{x})T}. \quad (\text{A.7})$$

Upper-bounding the 2-norm by the Frobenius norm and taking  $K = \sqrt{j(n-j)} \frac{\bar{a}\Delta T}{1-\alpha}$ , the bound in the theorem follows. This bound is conservative, due to the use of the Frobenius norm, but it shows the exponential rate of convergence. Using the bound (A.3), one can show that the sequence of iterates is Cauchy. Moreover this is true for every sufficiently small  $\Delta T$ . Because the space of  $j$ -dimensional subspaces in  $T_{\mathbf{x}}\mathbb{R}^n$ , a Grassmannian, with the distance given in (13) as the metric, is complete, we conclude that  $\mathcal{L}_j^+(T, \mathbf{x})$  approaches a fixed subspace. This subspace is  $\mathcal{L}_j^+(\mathbf{x})$  defined in Section 4.2, because all vectors in it have exponents less than or equal to  $\mu_j^+(\mathbf{x})$  and one can show that any vector not in the subspace must have a larger exponent. The proof for backward time is similar. ■

## Appendix B. Averaging Time Determination

In order to automate determining the averaging time for  $\mathbf{x}_j$  for the calculation of the FTLVs, the averaging time is iteratively increased, without restricting the forward and backward averaging times to be the same. For the computations in 7.4.2, for each pair  $(x_1, \lambda_1)$ , the value of  $(x_2, \lambda_2)$  approximating a point on the invariant center manifold is computed using an algorithm consisting of two nested iteration loops with  $i$  indicating the inner-loop iteration and  $k$  the outer-loop iteration, with  $i, k = 0, 1, 2, \dots$ . The variables and iteration indices follow the format:  $T_{fwd}^{(k)}, T_{bwd}^{(k)}, \mathbf{x}_j^{(i,k)}, x_2^{(i,k)}$ , and  $\lambda_2^{(i,k)}$ .

1. Initialization: Set  $\mathbf{x}_j^{(0,0)} = \mathbf{x}_j$  and  $(x_2^{(0,0)}, \lambda_2^{(0,0)})$  to the values of those coordinates in  $\mathbf{x}_j^{(0,0)}$ . Set  $T_{fwd}^{(0)} = \bar{T} = 0.5$  and  $T_{bwd}^{(0)} = \bar{T} = 0.5$ .
2. Inner-loop iteration  $i+1$  at outer iteration  $k$ : Calculate  $\mathbf{I}_1^-(T_{bwd}^{(k)}, \mathbf{x}_j^{(i,k)})$  and  $\mathbf{I}_4^+(T_{fwd}^{(k)}, \mathbf{x}_j^{(i,k)})$  and determine the values of  $x_2^{(i+1,k)}$  and  $\lambda_2^{(i+1,k)}$  that satisfy

$$\begin{aligned} \langle \mathbf{I}_1^-(T_{bwd}^{(k)}, \mathbf{x}_j^{(i,k)}), \mathbf{f}(\mathbf{x}_j^{(i+1,k)}) \rangle &= 0 \\ \langle \mathbf{I}_4^+(T_{fwd}^{(k)}, \mathbf{x}_j^{(i,k)}), \mathbf{f}(\mathbf{x}_j^{(i+1,k)}) \rangle &= 0. \end{aligned} \quad (\text{B.1})$$

For this example the unknowns appear linearly; thus analytical solutions for  $x_2^{(i+1,k)}$  and  $\lambda_2^{(i+1,k)}$  can be obtained. Iterate until the inner-loop stopping criteria are met. The stopping criteria consider the relative change in the dependent variables from the previous iteration and  $\theta^{(i+1,k)}$  is the

angle between  $\mathbf{f}(\mathbf{x}_j^{(i+1,k)})$  and its orthogonal projection in  $\mathcal{E}^c(T_{fwd}^{(k)}, T_{bwd}^{(k)}, \mathbf{x}_j^{(i,k)})$  according to

$$\begin{aligned} |x_2^{(i+1,k)} - x_2^{(i,k)}|/|x_2^{(i,k)}| &< \text{tol}_{x_2}, \\ |\lambda_2^{(i+1,k)} - \lambda_2^{(i,k)}|/|\lambda_2^{(i,k)}| &< \text{tol}_{\lambda_2}, \\ \theta^{(i+1,k)} &< \text{tol}_\theta. \end{aligned} \quad (\text{B.2})$$

For this example, we used  $\text{tol}_{x_2} = \text{tol}_{\lambda_2} = \text{tol}_\theta = 10^{-5}$ . The approximation at the end of the inner-loop is denoted by  $\hat{\mathbf{x}}_j^{(k)}$ .

3. Outer-loop iteration: Check the outer-loop stopping criterion

$$\|\hat{\mathbf{x}}_j^{(k)} - \hat{\mathbf{x}}_j^{(k-1)}\|_2 < \text{tol} \quad (\text{B.3})$$

We used  $\text{tol} = 10^{-6}$ . When  $k = 0$ , we use  $\mathbf{x}_j$  in place of  $\hat{\mathbf{x}}_j^{(k-1)}$ . If the criterion is satisfied, stop and yield the final approximation  $\hat{\mathbf{x}}_j$  to the center manifold point for the pair  $(x_1, \lambda_1)$  under consideration. Otherwise perform the  $(k+1)^{\text{th}}$  outer-loop iteration with the averaging times

$$T_{fwd}^{(k+1)} = T_{fwd}^{(k)} + dT_{fwd}, \quad T_{bwd}^{(k+1)} = T_{bwd}^{(k)} + dT_{bwd}. \quad (\text{B.4})$$

We used  $dT_{fwd} = 0.3$  and  $dT_{bwd} = 0.1$ . With the new averaging times, repeat the inner-loop iterations starting with  $\hat{\mathbf{x}}_j^{(k)}$ .

The computations for the five points required about 5 inner iterations for each outer iteration and the forward and backward averaging times were increased to about 5.0 and 2.0 respectively. Experiments with initializing the iterative process with different dependent variable estimates consistently led to the same invariant center manifold point approximations.

## References

- [1] A. Adrover, S. Cerbelli and M. Giona, Exterior algebra-based algorithms to estimate Lyapunov spectra and stretching statistics in high-dimensional and distributed systems, *International Journal of Bifurcation and Chaos* 12(2) (2002) 353–368.
- [2] A. Adrover, F. Creta, M. Giona, M. Valorani and V. Vitacolonna, Natural tangent dynamics with recurrent biorthonormalizations: A geometric computational approach to dynamical systems exhibiting slow manifolds and periodic/chaotic limit sets, *Physica D* 213(2) (2006) 121–146.
- [3] A. Adrover, F. Creta, M. Giona, and M. Valorani, Stretching-based diagnostics and reduction of chemical kinetic models with diffusion, *J. Computational Physics* 225 (2007) 1442–1471.
- [4] E. Aykutluğ and K. D. Mease, Approximate Solution of Hypersensitive Optimal Control Problems Using Finite-Time Lyapunov Analysis, *American Control Conference*, St. Louis, Missouri, June 2009.
- [5] L. Barreira and Y. B. Pesin, *Lyapunov Exponents and Smooth Ergodic Theory*, University Lecture Series, Vol. 23, American Mathematical Society, Providence, 2002.
- [6] M. Branicki, A. M. Macho, and S. Wiggins, A Lagrangian description of transport associated with a front-eddy interaction: Application to data from the North-Western Mediterranean Sea, *Physica D* 240 (2011) 282–304.
- [7] H. W. Broer, A. Hagen, and G. Vegter, Numerical continuation of normally hyperbolic invariant manifolds, *Nonlinearity* 20 (2007) 1499–1534.
- [8] R. Buizza and T. N. Palmer, The singular-vector structure of the atmospheric global circulation, *J. Atmos. Sci.* 52(9) (1995) 1434–1456.
- [9] E. Chiavazzo, A. N. Gorban, and I. V. Karlin, Comparison of invariant manifolds for model reduction in chemical kinetics, *Communications in Computational Physics* 2 (2007) 964992.

- [10] M. J. Davis and R. T. Skodje, Geometric investigation of low-dimensional manifolds in systems approaching equilibrium, *J. Chemical Physics* 111 (1999) 859–874.
- [11] L. Dieci and E. S. Van Vleck, Lyapunov spectral intervals: theory and computation, *SIAM J. Numerical Analysis* 40(2) (2002) 516–542.
- [12] R. Doerner, B. Hübinger, W. Martienssen, S. Grossmann, and S. Thomae, Stable manifolds and predictability of dynamical systems, *Chaos, Solitons, and Fractals* 10(11) (1999) 1759–1782.
- [13] J.P. England, B. Krauskopf, and H.M. Osinga, Computing two-dimensional global invariant manifolds in slow-fast systems, *Int. J. Bifurcation and Chaos* 17(3) (2007) 805–822.
- [14] S. V. Ershov and A. B. Potapov, On the concept of stationary Lyapunov basis, *Physica D* 118 (1998) 167–198.
- [15] N. Fenichel, Geometric singular perturbation theory for ordinary differential equations, *J. Differential Equations* 31 (1979) 53–98.
- [16] C. Froeschle, E. Lega and R. Gonczi, Fast Lyapunov indicators: application to asteroidal motion, *Celestial Mechanics and Dynamical Astronomy* 67 (1997) 41–62.
- [17] C. W. Gear, T. J. Kaper, I. G. Kevrekidis, and A. Zagaris, Projecting to a slow manifold: Singularly perturbed systems and legacy codes, *SIAM J. Applied Dynamical Systems* 4 (2005) 711732.
- [18] K. Geist, U. Parlitz and W. Lauterborn, Comparison of different methods for computing Lyapunov exponents, *Progress of Theoretical Physics* 83(5) (1990) 875 – 893.
- [19] I. Goldhirsch, P.-L. Sulem, and S. A. Orszag, Stability and Lyapunov stability of dynamical systems : a differential approach and a numerical method, *Physica D* 27 (1987) 311–337.
- [20] G. H. Golub and C. F. Van Loan, *Matrix Computations*, 3rd Edition, The Johns Hopkins University Press, Baltimore, 1996.
- [21] J. M. Greene and J.-S. Kim, The calculation of Lyapunov spectra, *Physica D* 24(1-3) (1987) 213–225.
- [22] J. M. Greene and J.-S. Kim, Introduction of a metric tensor into linearized evolution equations, *Physica D* 36 (1989) 83–91.
- [23] J. Guckenheimer and C. Kuehn, Computing slow manifolds of saddle type, *SIAM J. Appl. Dyn. Syst.* 8(3) (2009) 854–879.
- [24] G. Haller, Finding finite-time invariant manifolds in two-dimensional velocity fields, *Chaos* 10(1) (2000) 99–108.
- [25] G. Haller, A variational theory of hyperbolic Lagrangian coherent structures, *Physica D* 240 (2011) 574–598.
- [26] A. Hammerlindl, Integrability and Lyapunov exponents, *J. Modern Dynamics* 5(1) (2011) 107–122.
- [27] B. Hasselblatt and Y. B. Pesin, Partially Hyperbolic Dynamical Systems, in B. Hasselblatt and A. Katok (Eds.), *Handbook of Dynamical Systems*, Vol. 1B, Elsevier, New York, 2005.
- [28] H. W. Hirsch, M. Shub, and C. C. Pugh, *Invariant Manifolds*, Springer-Verlag, New York, 1977.
- [29] A. Isidori, *Nonlinear Control Systems*, 3rd Edition, Springer-Verlag, New York, 1995 21.
- [30] C. K. R. T. Jones, Geometric Singular Perturbation Theory, in R. Johnson (Ed.), *Dynamical Systems, Lecture Notes in Math* 1609, Springer, Berlin, 1995.
- [31] H. G. Kaper and T. J. Kaper, Asymptotic analysis of two reduction methods for systems of chemical reactions, *Physica D* 165 (2002) 66–93.
- [32] A. Katok and B. Hasselblatt, *Introduction to the Modern Theory of Dynamical Systems*, Cambridge University Press, New York, 1995.
- [33] P. V. Kokotovic, H. K. Khalil, and J. O'Reilly, *Singular Perturbation Methods in Control: Analysis and Design*, Academic Press, New York, 1986.
- [34] S. H. Lam, Singular perturbation for stiff equations using numerical computations, *Lectures in Applied Mathematics* 24 (1986) 3–19.
- [35] S. H. Lam and D. A. Goussis, The CSP method for simplifying kinetics, *Int. J. Chemical Kinetics* 26 (1994) 461–486.
- [36] G. Lapeyre, Characterization of finite-time Lyapunov exponents and vectors in two-dimensional turbulence, *Chaos* 12(3) (2002) 688–698.
- [37] B. Legras and R. Vautard, A guide to Lyapunov vectors, in: *Predictability*, Vol. 1, ed. T. Palmer, ECWF Seminar, Reading, UK, 1996 135–146.
- [38] F. Lekien and S. D. Ross, The computation of finite-time Lyapunov exponents on unstructured meshes and for non-Euclidean manifolds, *Chaos* 20 (2010) 20 pages.
- [39] E. N. Lorenz, The local structure of a chaotic attractor in 4-dimension, *Physica D* 13 (1984) 90–104.
- [40] A. M. Lyapunov, The general problem of stability of motion, *Intern. J. of Control*, 55(3) (1992) 531–773. (reprint of Lyapunov's 1892 Thesis)
- [41] U. Maas and S. B. Pope, Simplifying chemical kinetics: intrinsic low-dimensional manifolds in composition space, *Combustion and Flame* 88 (1992) 239–264.
- [42] K. D. Mease, Geometry of computational singular perturbations, in *Nonlinear Control System Design*, Vol. 2, A. J. Krener and D. Q. Mayne, Oxford, UK, Pergamon, 1996 855–861.
- [43] K. D. Mease, S. Bharadwaj, and S. Iravanchy, Timescale analysis for nonlinear dynamical systems, *J. Guidance, Control and Dynamics* 26 (2003) 318–330.
- [44] K. D. Mease, Multiple timescales in nonlinear flight mechanics: diagnosis and modeling, *Applied Mathematics and Computation* 164 (2005) 627–648.
- [45] J. Nafe and U. Maas, A general algorithm for improving ILDMs, *Combustion Theory Modelling* 6 (2002) 697–709.
- [46] D. S. Naidu and A. J. Calise, Singular perturbations and timescales in guidance and control of aerospace systems: a survey, *J. Guidance, Control and Dynamics* 24(6) (2001) 1057–1078.
- [47] R. E. O'Malley, *Singular Perturbation Methods for Ordinary Differential Equations*, Springer-Verlag, New York, 1991.
- [48] V. Oseledec, A multiplicative ergodic theorem: Lyapunov characteristic numbers for dynamical systems, *Trans. Moscow Math. Soc.* 19 (1968) 197–231.
- [49] A. V. Rao and K. D. Mease, Dichotomic basis approach to solving hyper-sensitive optimal control problems, *Automatica* 35 (1999) 633–642.
- [50] A. V. Rao and K. D. Mease, Eigenvector approximate dichotomic basis method for solving hyper-sensitive optimal control problems, *Optimal Control Applications and Methods* 21 (2000) 1–19.
- [51] B. Rasmussen and L. Dieci, A geometrical method for the approximation of invariant tori, *J. Computational and Applied Mathematics* 216 (2008) 388–412.
- [52] Z. Ren and S. B. Pope, The geometry of reaction trajectories and attracting manifolds in composition space, *Combustion Theory and Modeling* 10(3) (2006) 361–388.
- [53] M. R. Roussel and S. J. Fraser, Geometry of the steady-state approximation: perturbation and accelerated convergence methods, *J. Chem. Phys.* 93(3) (1990) 1072–1081.
- [54] B. Sandstede, S. Balasuriya, C. K. R. T. Jones, and P. Miller, Melnikov theory for finite-time vector fields, *Nonlinearity* 13 (2000) 1357–1377.
- [55] P. J. Schmid, Nonmodal Stability Theory, *Annu. Rev. Fluid Mech.* 39 (2007) 129–162.
- [56] L. A. Segel and M. Slemrod, The Quasi-Steady-State assumption: a case study in perturbation, *SIAM Review* 31(3) (1989) 446–477.
- [57] S. C. Shadden, F. Lekien, and J. E. Marsden, Definition and properties of Lagrangian coherent structures from finite-time Lyapunov exponents in two-dimensional aperiodic flows, *Physica D* 212 (2005) 271–304.
- [58] S.-K. Tin, N. Kopell, and C. K. R. T. Jones, Invariant manifolds and singularly perturbed boundary value problems, *SIAM J. Numer. Anal.* 31 (1994) 1558–1576.
- [59] J. A. Vastano and R. D. Moser, Short-time Lyapunov exponent analysis and the transition to chaos in Taylor-Couette flow, *J. Fluid Mechanics* 233 (1991) 83–118.
- [60] B. F. Villac, Using FLI maps for preliminary spacecraft trajectory design in multi-body environments, *Celestial Mechanics and Dynamical Astronomy* 102(1-3) (2008) 29–48.
- [61] C. L. Wolfe and R. M. Samelson, An efficient method of recovering Lyapunov vectors from singular vectors, *Tellus* 59A (2007) 355–366.
- [62] S. Yoden and M. Nomura, Finite-time Lyapunov stability analysis and its application to atmospheric predictability, *J. Atmospheric Sciences* 50(11) (1993) 1531–1543.
- [63] L.-S. Young, Ergodic Theory of Differentiable Dynamical Systems, in: *Real and Complex Dynamics*, eds. Branner and Hirth, NATO ASI Series, Kluwer Academic Publishers, 1995 201–226.
- [64] A. Zagaris, H. G. Kaper and T. J. Kaper, Analysis of the computational singular perturbation reduction method for chemical kinetics, *J. Nonlinear Sci.* 14 (2004) 59–91.